ASTRONOMY & ASTROPHYSICS
SUPPLEMENT SERIES

Astron. Astrophys. Suppl. Ser. **126,** 281-296 (1997)

The solar disk spectrum between 660 and 1175 Å (first order) obtained by SUMER on SOHO⋆

W. Curdt[1], U. Feldman[2], J.M. Laming[3], K. Wilhelm[1], U. Schühle[1], and P. Lemaire[4]

[1] Max-Planck-Institut für Aeronomie, D-37191 Katlenburg-Lindau, Germany
[2] Naval Research Laboratory, Washington, D.C., U.S.A.
[3] SFA Inc, 1401 McCormick Drive, Largo, MD 20774 and Naval Research Laboratory, Washington, D.C., U.S.A.
[4] Institut d'Astrophysique Spatiale, Unité Mixte, CNRS-Université Paris XI, Bat 121, F-91405 Orsay, France

Received December 10, 1996; accepted March 18, 1997

Abstract. SUMER – Solar Ultraviolet Measurements of Emitted Radiation – onboard of SOHO – Solar and Heliospheric Observatory – obtained its first spectrum on January 25, 1996 near the north polar limb. The range from 660 Å to 1175 Å which has never before been observed with such a good spectral resolution contains a wealth of spectroscopic details. Identification of about 400 lines in this spectral range is given. We list the wavelengths of identified transitions and provide their absolute peak intensities. General spectral features of the most abundant elements H, He, C, N, O, Ne, Mg, Si, S, Ar, and Fe are described. In this spectral range many density- and temperature-sensitive line pairs are found. It is shown in examples how they can be used as diagnostic tools.

Key words: Sun: atmosphere — chromosphere — transition region — UV radiation

1. Introduction

The first spectrum of the Sun with SUMER was obtained near the north polar limb on January 25, 1996 between $10:52-12:08$ UT. Sections of the northern polar coronal hole and the limb were covered as well as the lower corona on the off-limb section of the slit. We present here the analysis of a portion of this spectrum ranging from its lower limit around 660 Å to the C III multiplet around 1175 Å in first order. Second order lines are superimposed on this spectrum. The upper limit of the list of identified lines was chosen as many detailed spectral studies above this value have already been performed using Skylab and HRTS data (Brekke et al. 1991; Sandlin et al. 1986; Cohen et al. 1978) and thus the need to study the SUMER data was not so urgent for longer wavelengths. Many other spectra from different regions of the Sun have been obtained since the first light spectrum, but are not subject of this communication.

The high temperature solar atmosphere is the only astrophysical plasma source that can be studied with high spatial resolution. Much of our understanding of stellar atmospheres is based on the understanding of plasma processes that occur in the upper solar atmosphere. Although some of the plasma processes can be studied by high-resolution images of the solar atmosphere much of our knowledge on temperatures, densities, emission measures, mass motions and elemental abundances comes from high-resolution spectral observations in the range from the far ultraviolet (VUV) to X-ray wavelengths ($2000 - 1.7$ Å), a range that is not accessible by groundbased observations. During the past 40 years much progress has been made in solar high resolution spectroscopy from space (see Feldman et al. 1988). During the 1960's, a group in Culham launched several rocket-borne high-resolution spectrometers to record the solar spectrum which also included wavelengths short of 1175 Å. This spectral range was also covered by the Skylab ATM experiment with modest spectral resolution ($1 - 3$ Å). Line lists and identifications containing some of the most prominent lines in this region were published (Burton & Ridgeley 1970; Vernazza & Reeves 1978; Noyes et al. 1985).

The very high normal-incidence reflectivity of aluminum-coated optics at wavelengths longer than 1175 Å made it possible to construct multi-element instruments which combine high spectral and spatial resolution resulting in detailed observations of the solar spectrum in this wavelength range. Utilizing these observations a number of line lists were compiled of which the most comprehensive are the lists by Sandlin et al. (1986) and

Send offprint requests to: W. Curdt (Curdt@linmpi.mpg.de)

⋆ Table 1 and Fig. 4 are also available in digital form at the CDS via anonymous ftp to cdsarc.u-strasbg. fr (130.79.128.5) or via http://cdsweb.u-strasbg.fr/Abstract.html

Cohen et al. (1978). The wavelength region between 660 and 1175 Å remained poorly observed. One of the instruments on Skylab was a high-resolution normal-incidence spectrometer (S082 B) constructed by the Naval Research Laboratory (Bartoe et al. 1977). Although the optics of the S082 B instrument were $Al + MgF_2$ coated, a few very long observations of bright solar features resulted in useful spectra at wavelengths as short as 970 Å. A line list compiled from these observations was published by Feldman & Doschek (1991).

2. Instrument and data acquisition

This section describes the data acquisition and instrumental details which are relevant for the interpretation of the data. A more detailed instrument description is given by Wilhelm et al. (1995) and first inflight performance characteristics are given by Wilhelm et al. (1997a) and Lemaire et al. (1997). SUMER is a stigmatic normal-incidence spectrograph operating in the range from 400 to 1610 Å with mirrors made out of SiC and three normal-incidence reflexions. The steep fall-off of the reflectivity below 500 Å determines the lower wavelength limit. Only few lines short of 500 Å have been identified so far.

The off-axis parabola telescope mirror has a focal length of 1302.77 mm. It can be moved in two dimensions around the focal point to allow pointing of the instrument in the range of ±32 arcmin. This allows us to take disk and off-limb spectra in the lower corona.

Four spectrometer slits with angular dimensions of 4×300, 1×300, 1×120, and 0.3×120 arcsec^2 are available. The slit assembly allows us to move a selected slit into the telescope focus and to refocus its position if required. With the slit the photon input for the detector can be adjusted according to the selected spectral band and to the solar feature observed. The measurements in this communication were performed with the 0.3×120-arcsec slit, and the widths of the spectral lines thus are not affected by the slit width.

Two diffraction orders can be observed by SUMER; first order lines and second order lines appear superimposed in the SUMER spectrum. The dispersion of the spectrometer varies slightly with wavelengths from 45 mÅ/pixel (first order) and 22.5 mÅ/pixel (second order) at 800 Å to 41.8 mÅ/pixel and 20.9 mÅ/pixel at 1600 Å.

The instrument is equipped with two photon-counting detectors (A and B) operating in Cross Delay Line technique (XDL) – for details see Siegmund et al. (1994). Only one detector can be operated at a time. Each detector has 1024 spectral pixels and 360 spatial pixels. The pixel size of approximately 26.5 μm × 26.5 μm is defined by the analogue electronics. The central area of the detector is coated with KBr while both sides are bare microchannel plate (cf., Fig. 1).

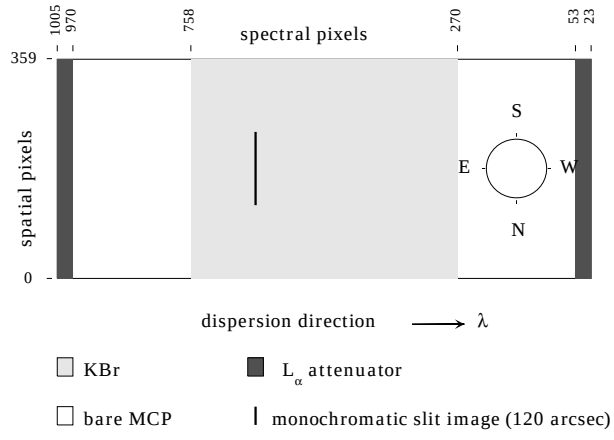

Fig. 1. Detector B photocathode layout (view from grating to the focal plane). The limb spectrum discussed in this paper was obtained with a short slit covering only 120 pixels. Each individual spectrum extends for approximately 45 Å (1st order) in the dispersion direction. Some pixels on either side are dark

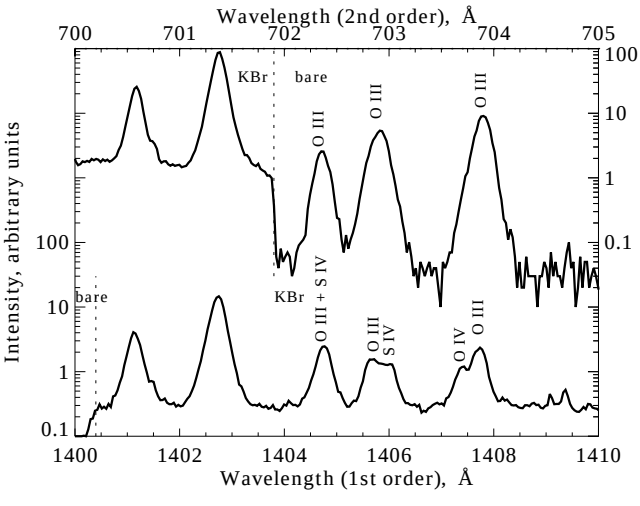

Fig. 2. The limb spectrum around 703 Å (2nd order) on both sections of the detector photocathode. The O III lines at 702.332, 702.899, and 703.85 Å are blended with S IV (1404.77, 1406.06 Å), and O IV (1407.386 Å) lines, if recorded on the KBr coating (bottom). On the bare part (top), the O III triplet is prominent

The KBr coating increases the detective quantum efficiency (DQE) up to a factor of > 10 in the range from 900 Å to 1500 Å. Observation of lines in both sections of the photocathode helps to detect second order lines, since they appear in similar intensity on both parts of the photocathode. This effect is demonstrated in Fig. 2.

Only a few second order lines have been identified in the spectral range below 590 Å where the instrument sensitivity is very low, whilst corresponding first order lines fall into the efficiency maximum. He I at 584 Å is the most

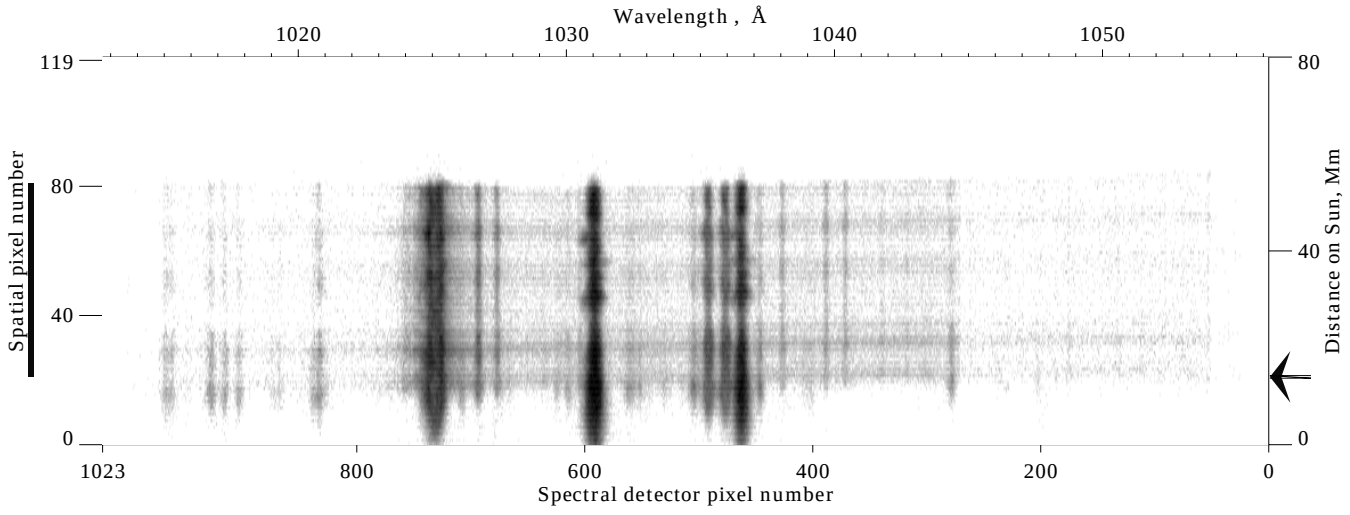

Fig. 3. Detector image centered around 1035 Å. This individual spectrum is dominated by the O VI resonance lines and the H I Ly$_\beta$ line which is broad and shows self-absorption. The position of the photospheric limb is marked (North is down) and the selected range along the slit is indicated by a bar. Note, that the image of the slit was not yet well adjusted at that time

prominent second order line in the spectrum presented here.

The spectra presented in this communication were taken with detector B. The spectral ranges of both detectors are different; the B detector range reaches from 330 to 750 Å in second order and 660 to 1500 Å in first order. The range from 660 to 750 Å is covered twice. From the line ratio of the O III line at 703.85 Å in both orders a grating efficiency ratio between first and second order of 1.0 was obtained.

During the laboratory calibration (Hollandt et al. 1996) the SUMER instrument with both detectors was radiometrically calibrated against a secondary standard light source. In-flight calibration measurements with detector A indicate that this calibration is still valid within $\pm 15\%$ ($1\,\sigma$) (Wilhelm et al. 1997b). The detector B efficiency curve has not yet been validated under operational conditions. We have no indications for differences in the performance of detector B and applied the laboratory efficiency curve for this analysis. Below 769 Å this curve had to be extrapolated, and progressively increasing uncertainties have to be assumed.

Both detectors show non-uniformity effects typical for MCP intensifiers. These effects stem from the MCP structure, the inhomogeneity of the HV electric field, and individual pixel errors. These effects, which are very worrisome for imaging purposes can be compensated to a large extent by a flat field correction; SUMER regularly generates a flat-field matrix which can be applied either on board, or on the ground. The dark signal of the detectors is extremely low and for disk observations scattered light is irrelevant. Thus, it is inferred that continuum contributions of the spectra have a solar origin.

Bright spectral lines, if placed onto the KBr part of the photocathode lead to a local gain depression even if the narrow slit is used. As a result the DQE of the detector can decrease locally and peak intensities might be attenuated in a non-linear fashion (Wilhelm et al. 1997a). This effect starts at 10 cts/pixel/s and deteriorates progressively. No corrections have been performed for local gain depression effects, although the intense lines of C III (977 Å), H I Lyβ (1025 Å), O VI (1032 Å), O VI (1036 Å) are affected to some extent.

For the spectrum, taken on January 25, 1996, the instrument was pointing towards the solar limb at the North pole of the Sun (cf., Fig. 3). With the given slit of 0.3×120 arcsec only a window of 1024 by 120 pixels is read out by the detector. At that time, the slit image was not yet adjusted with respect to the read-out window, leaving ~ 30 pixels unexposed. The remaining 90 pixels cover approximately 60 arcsec of the northern coronal hole portion of the solar disk and about 30 arcsec beyond the photospheric limb. A set of 41 spectral sections, each offset by 17.4 Å and with a 40 Å gap around H I Ly α (introduced for safety reasons in this first spectrum) was exposed during this observation with increasing wavelength. The exposure time for individual spectra was 100 s. For this communication 29 exposures have been analysed. In total, 51 minutes elapsed between the first spectrum, taken around 680 Å, and the last spectrum considered here. The individual spectra have been corrected for minor telemetry errors.

3. The line list

As described in Sect. 2, each of the individual spectra consists of a two dimensional array of 120×1024 pixels. For line identification purposes, we have collapsed the two

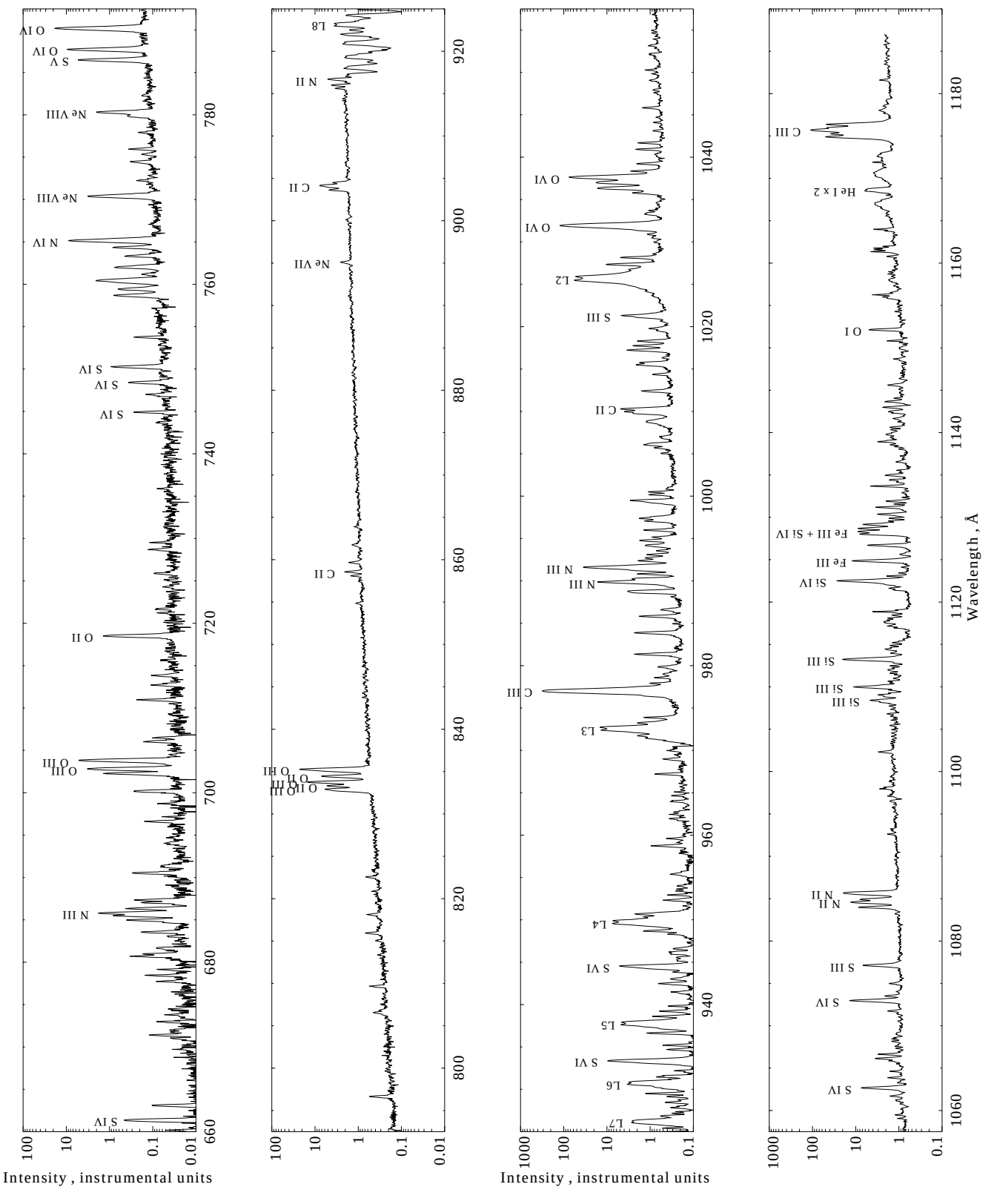

Fig. 4. Near-limb quiet-Sun composite spectrum recorded on January 25, 1996 near the solar North pole. The most prominent lines are labelled. Intensities are given in instrumental units

dimensional image array into a vector of intensity versus wavelength. Due to the stigmatic properties of SUMER, there is a one to one correspondence between the brightness along a spectral line image and the image of the solar atmosphere in the particular wavelength. Thus, the sections of the spectral line emitted from the chromospheric network boundaries are much brighter than those emitted from cell interiors. The position of the limb was determined from the continuum intensity fall-off. We have integrated over 60 pixels just inside the limb. For these pixels the line-of-sight is almost tangential to the solar surface and the effect of limb-brightening is seen in many hot spectral lines. Figure 4 is a display of the averaged composite spectrum presented in this paper. The count rates of this average spectrum have been radiometrically calibrated and are given as absolute intensities in column one of Table 1. These peak intensities are meant as a first assessment of absolute line strengths. Absolute line intensities – sorted by solar features and with blends separated – are deferred to a later communication.

We have found that the dispersion of pixels $100-800$ of detector B is linear to better than 0.02 Å. Figure 5 displays the dispersion of the spectrometer on detector B for three different wavelength positions. Notice that the uncertainties in determining the wavelengths are generally 0.02 Å or better. SUMER wavelength measurements were determined as follows: The positions of the centroids of all spectral features in the $100-800$ pixel range were measured visually. Using several of the well-established wavelengths as standards we have calculated the wavelengths of all the lines in the image using a first order polynomial fit programme. The reference lines (preferably cold chromospheric lines) for the wavelength calibration are marked by an asterisk in Table 1. A comparison between measured and known wavelengths suggests that, on the average, the wavelengths for unblended lines were determined to about 0.02 Å. Column two of Table 1 lists the wavelengths available in the literature and column three lists the measured wavelengths. The vast majority of the laboratory wavelengths for column two, and identifications listed in column four and five are from Kelly (1987). Wavelengths of unidentified lines measured on the SUMER plots are also included in the table.

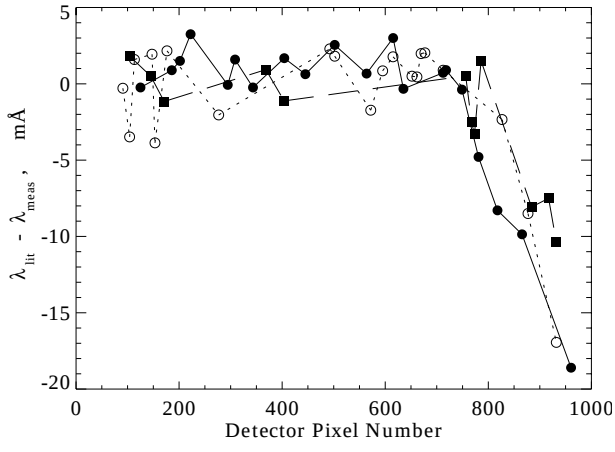

Fig. 5. Uniformity of the dispersion along the spectral dimension of detector B for three different wavelength positions. For pixels $150-800$, the scatter is less than 0.005 Å and thus the accuracy of the wavelength determination is at least 0.02 Å

4. Comments on some of the lines in the list

The first light spectrum – recorded with the high spectral resolution and the excellent dynamic range available to SUMER – reveals many spectral details and accommodates many more spectral lines than given in any earlier line list. Although some of the lines suggested earlier could not be identified. This near-limb disk spectrum of the quiet Sun in the $660-1175$ Å spectral range is dominated by lines emitted from temperatures typical of the chromosphere and the transition region. Only the most intense coronal lines are visible in a quiet Sun spectrum recorded on the disk. The strength of coronal lines when compared to the transition region lines should increase in the vicinity of the solar limb. The actual widths of most of the lines in the list is larger than the instrumental width. In principle, SUMER can separate lines such as C II at 903.96 and 904.14 Å (Wilhelm et al. 1997a), which are offset by only 0.18 Å. On the limb, lines are indeed wider and as a result, two lines that are separated from each other by less than 0.3 Å appear as a blend. In places where blends are expected we have provided the wavelengths and the transitions of some of the most prominent lines expected in the blend. Below we give an account of some interesting line systems presented in the list.

Hydrogen

The hydrogen Lyman series lines are very prominent in the spectral range covered by SUMER. The transition of the highest member of the series that can be distinguished in the spectrum used for this identification is $1s-18p$. The higher members of the Lyman series are blended with the hydrogen free bound continuum. Line shapes of most, if not all, the hydrogen lines are dominated primarily by opacity effects and to a lesser degree by the Doppler nonthermal mass motions. In spectra obtained from regions where opacity effects are reduced several additional members of the Lyman series can be distinguished, (Wilhelm et al. 1997a).

Helium

The 584.33 Å $1s^2\ {}^1S_0-1s2p\ {}^1P_1$ line in second order is the only He I line visible in this quiet Sun spectrum. He II multiplets of the type $2k-nk'$ (Balmer series) where $n>4$, are present in the observed range. Individual lines within each multiplet are not resolved in the SUMER spectrum. The

He II multiplets arising from transitions with even "n" quantum numbers have wavelengths that are about 0.4 Å shorter than hydrogen Lyman series lines. Therefore, because of the very large widths of the hydrogen lines in this limb spectrum, the He II transitions are visible but blended with the blue wings of the hydrogen lines. The He II Balmer lines belonging to transitions having odd upper quantum members (i.e., n = 5, 7 and 9) are well observed in our spectrum.

The excitation energy of the He II Balmer lines is $\approx$ 50 eV while their formation temperature, assuming collisional excitation, is only equivalent to about 10 eV. As a result, the Boltzmann factors that determine the rate of collisional excitation processes in these lines are very temperature sensitive. He II line intensities when compared to the intensities of other lines emitted by plasmas with similar temperatures, are good indicators for the excitation processes taking place in the quiet Sun atmosphere (Feldman 1995).

Carbon

The series limit of the C I $2s^22p^2\ ^3P-2s^22pnk$ is at 1101 Å. Therefore, wavelengths slightly longer than the series limit are abundant with lines belonging to high members of the CI Rydberg series. The line list contains many C I lines belonging to transitions between the $2s^22pnd$ upper configurations (where n = 6, 7, ... 13) and the ground term $2s^22p^2\ ^3P$. The $2s^22p^2\ ^3P - 2s2p^3\ ^3S$ multiplet of C I at 945 Å is also present in this limb spectrum.

The ground term of C II is $2s^22p\ ^2P$ and the first excited configuration $2s2p^2$ include, in order of increasing energies, the ^4P, ^2D, ^2S, and ^2P terms. The lowest ^4P term can be regarded as metastable in electron density conditions typical to quiet Sun plasmas. Transitions between the excited doublets and the ground term appear in the SUMER spectrum. The lowest energy transitions are near 1330 Å and the two higher energy transitions are near 1037 and 904 Å. The three sets of C II transitions are among the brightest emitted by the chromosphere. Three lines belonging to transitions between the $2p^3\ ^4S$ and the metastable $2s2p^2\ ^4P$ term that appear near 1010 Å are also intense. Several more C II lines belonging to transitions between the ground term and doublet terms from highly excited configurations are present in the wavelength range. Intensity ratios between lines belonging to quartet and doublet systems can provide information regarding the temperature properties of the chromosphere plasmas.

The 977 Å C III $2s^2\ ^1S_0 - 2s2p\ ^1P_1$ transition is extremely bright in the quiet Sun spectrum. It is the strongest line emitted in the wavelength range discussed in this paper.

Nitrogen

The N I transitions between ground configuration levels ($2s^22p^3$) and levels from the excited configurations fall in the 950 – 1150 Å wavelength range. There are no N I lines resulting from transitions between excited configurations visible in this limb spectrum used to create the line list. The situation with N II is similar to the situation in N I. Some of the strongest transitions between the ground configuration $2s^22p^2$ and the excited configuration are present in this spectrum. The N II transitions appear near 671, 746, 915, and 1085 Å. There are no N II transitions arising from levels between excited configurations among the lines observed in the quiet Sun spectrum.

Resonance lines between the ground and excited configuration and lines between the first and second excited configurations in N III are observed near 690, 772, 980 and 990 Å while the N IV transitions appear near 765, 923, and 955 Å. Intensity ratios between the two types of lines are temperature sensitive. Intensity ratios among some of the lines near 923 arising from transitions between the first and second excited configurations are also sensitive to electron density conditions present in the quiet Sun.

Oxygen

A well known resonance exists between the 1s – 3p transition in H I (1026 Å) and the $2s^22p^4\ ^3P - 2s^22p^33d\ ^3D$ in O I. As a result the excited term 3d ^3D in part is photo-pumped by H I 1s – 3p photons causing transitions between it and lower energy levels to become unusually bright. Because of the very large widths of all the Lyman series lines coincidences between many of them and between O I lines from higher "n" values occur. As a result, H I lines photo-pump many O I levels which in turn cause many of the O I lines to become very prominent.

Several allowed transitions between the ground configuration and the first excited configuration in O II and O III are prominent in this SUMER spectrum. Two O IV lines belonging to transitions between $2s^22p\ ^2P - 2s2p^2\ ^2D$ appear at 787 and 790 Å. Additional O IV lines belonging to $2s2p^2\ ^2D - 2p^3\ ^2D$ appear at 779 Å. The relative intensities between the two sets of lines can be used as electron temperature indicators for the O IV formation region.

The $2s2p\ ^3P - 2p^2\ ^3P$ transitions of O V appear near 760 Å. The intensities of lines originating from the $2p^2\ ^3P_1$ level are sensitive to quiet Sun type densities when compared to the intensity from lines originating from the $2p^2\ ^3P_0$ or from the $2p^2\ ^3P_2$ levels. The O VI resonance lines at 1031.924 and 1037.614 Å are among the brightest emitted by upper transition region plasmas.

Neon

Lines emitted by neutral neon, Ne I, and by several neon ions are present in this limb spectrum. The two Ne I resonance lines at 735.896 and 743.720 Å, which belong to transitions between the first excited configuration $2s^22p^53s$ and the ground configuration $2s^22p^6$ are present in the spectrum though they are quite faint. No Ne II,

Ne III or Ne IV lines are visible in the 660 – 1150 Å range SUMER disk spectrum. The $2s^2 2p^2\ ^3P_1 - 2s2p^3\ ^5S_2$ Ne V transition at 1136.51 Å and the $2s^2 2p^2\ ^3P_2 - 2s2p^3\ ^5S_2$ transition at 1145.61 Å which is expected to be about three times brighter can be identified.

The Ne VI lines belonging to the $2s^2 2p\ ^2P - 2s2p^2\ ^4P$ transitions near 1000 Å appear with medium brightness. Several of the Ne VI transitions are blended with nearby lines. Lines belonging to the same transitions in N III and O IV are used as electron density indicators in quiet and active region plasmas. The Ne VI lines are sensitive to fairly high electron densities (larger than 5 10^{11} cm^{-3}) they will be good electron density indicators in unusually dense active region plasmas or in flares. The two 2s – 2p Ne VIII resonance lines in the SUMER spectral range represent the upper transition region type plasmas.

Magnesium

Lines from magnesium ions, at best, are poorly represented in this SUMER 660 – 1175 Å limb spectrum. Only the 3s – 6p 946.70 Å Mg II line may be present in the spectrum but cannot be identified without ambiguity.

Silicon

Many lines from Si III and Si IV are found in this spectrum. The Si III lines near 995 and 1108 Å belong to transitions between the first excited configuration 3s3p and the excited configurations 3s3d and 3s4s. Assuming that the opacity of Si III 1206.510 Å ($3s^2\ ^1S_0\ 3s3p\ ^1P_1$) resonance line, also in the SUMER range, can be determined, the relative intensities between these lines and the resonance line, could be used as density indicators. A number of Si IV lines near 1122 and 816 Å belonging to transitions between the first excited configuration 3p and the excited configurations 3d and 4s, and the 1066 Å line between the second excited configuration 3d and the 4f configuration are also present in the 660 – 1150 Å range. As in the Si III case the relative intensities between these transitions and the Si IV resonance lines 3s – 3p near 1400 Å which is also in the SUMER range can be used for electron temperature determination.

Sulfur

S I to S VI lines are numerous in the quiet Sun spectrum. The S I lines which appear in the 1050 – 1150 Å range are among the narrowest lines observed in the SUMER wavelength range. Lines of S II, S III and S IV between the ground configuration and several excited configurations are quite prominent. A number of S II lines appear in the 1000 – 1131 Å range. S III lines appear near 680, 700, 725, 1015, 1021 and 1077 Å and S IV lines appear near 750, 810 and 1070 Å. No transitions between excited configurations of S II, S III or S IV could be identified. The S V and S VI resonance lines and lines between the first and second excited configurations are also visible. Line ratios among some of these lines can be used for temperature diagnostic purposes. The S V lines appear near 696 and 780 Å and the S VI lines appear near 712, and very dominantly at 933 and 944 Å.

Argon

The abundance of argon in the solar atmosphere is more than 30 times lower than the abundance of neon. As a result lines emitted by argon ions are expected to be about an order of magnitude less intense when compared to lines of similar transitions emitted by neon ions. The Ar II $3s^2 3p^5\ ^2P - 3s3p^6\ ^2S$ transitions at 919.781 and 932.053 Å are expected to be present in this limb spectrum, however the 919.781 is blended with the red wing of the 919.351 Å H I line and with the 919.658 Å O I line. The 932.653 Å line similarly is blended with H I Ly 6.

The $3s^2 3p^2\ ^3P - 3s3p^3\ ^3P$ transitions near 720 Å range are the only Ar V lines visible in this spectrum. Because of the low argon abundance the lines are fairly faint. Two Ar VI lines at 767.06 and 1000.16 Å, belonging to transitions between $3s^2 3p - 3s3p^2$ levels may be associated with lines in our spectrum. The 3s – 3p Ar VIII lines at 700.245 and 713.812 Å, although fairly faint, probably are also present. The 700.245 Å line is blended with a nearby S III line. The Ar VIII lines are emitted from plasmas with temperatures of approximately of 4 10^5 K placing them among the hottest transition region lines in the list.

No transitions between the first and second excited configuration in argon ions are found in our spectrum. Thus, argon lines do not appear to be useful for temperature determinations or density diagnostics. However since argon is a high FIP (first ionisation potential) element, lines from argon ions can be used in conjunction with ions from low FIP elements to determine variations of elemental abundances in the upper solar atmosphere.

Iron

A large number of Fe III lines have been identified at wavelengths longer than 860 Å. The Fe III lines belong to transitions between levels of the first excited configuration $3s^2 3p^6 3d^5 4p$ and levels belonging to the $3s^2 3p^6 3d^6$ ground configuration. It is expected that many additional Fe III lines at wavelengths short of 860 Å should be present in the spectrum, but are not detected, because of the brightness of the Lyman continuum. No Fe II lines, which are quite plentiful in the longer wavelengths of the disk spectrum are undoubtedly identified in the wavelength range shorter than 1150 Å.

5. Spectroscopic diagnostics with SUMER

Numerous diagnostics for various plasma parameters are available in the spectra observed by SUMER. In this section we give examples of electron density and temperature

diagnostics, and a line intensity ratio that is suggestive of non-equilibrium effects.

Turning first to electron density measurements, we consider the intensity ratio

$$I\left(2s2p\ ^3P_0 - 2p^2\ ^3P_1\right) / I\left(2s2p\ ^3P_1 - 2p^2\ ^3P_0\right)$$

in the Beryllium-like sequence. In N IV these lines fall at 924.283 Å and 921.992 Å, and in O V at 759.441 Å and 761.128 Å respectively. For Gaussian line pairs with identical FWHM, peak intensity ratios can be taken. Taking level populations from Keenan et al. (1984) these ratios are plotted as a function of density in Figs. 6 and 7.

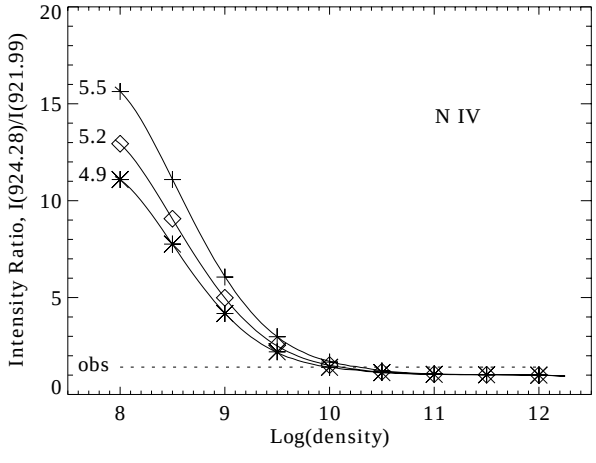

Fig. 6. Plot of the intensity ratio $I(924.28)/I(921.99)$ of N IV as a function of density, in photon units, for logarithmic electron temperatures of 4.9, 5.2, and 5.5, indicated by the three solid lines. The observed ratio, 1.4, is shown by the dotted line, and indicates densities of just greater than 10^{10} cm^{-3}, depending slightly on the assumed temperature

Curves are given for the temperature at which these ions have their maximum fractional abundance as given by Arnaud & Rothenflug (1985), and for temperatures a factor of two above and below these. As can easily be seen, the O V ratio allows a density of about 8 10^9 cm^{-3} to be inferred, while the N IV ratio suggests 1.4 10^{10} cm^{-3}. Hence both ratios are consistent with a pressure of $\sim$ 2 10^{15} cm^{-3} K. Electron density diagnostics at higher temperature are available in the spectrum of Ne VI, in the $2s^2 2p\ ^2P - 2s2p^2\ ^4P$ multiplet with lines around 1000 Å (see Keenan et al. 1994 for a detailed description).

Temperature diagnostics are available in the ratio

$$I\left(2s2p^2\ ^2D_{5/2} - 2p^3\ ^2D_{5/2}\right) / I\left(2s^2 2p\ ^2P_{1/2} - 2s2p^2\ ^2D_{3/2}\right)$$

in the Boron-like sequence. Taking electron impact excitation rates from Stafford et al. (1994) for N III and Zhang et al. (1994) for O IV, A-coefficients from Nussbaumer & Storey (1979) for N III and Nussbaumer & Storey (1982) for O IV, supplemented by values from Dankwort

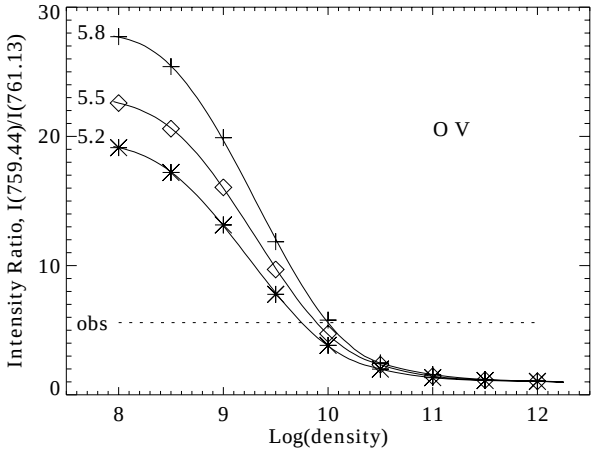

Fig. 7. Plot of the intensity ratio $I(759.44)/I(761.13)$ of O V as a function of density, in photon units, for logarithmic electron temperatures of 5.2, 5.5, and 5.8, indicated by the three solid lines. The observed ratio, 5.6, is shown by the dotted line, and indicates densities of just less than 10^{10} cm^{-3}, depending slightly on the assumed temperature

& Trefftz (1978) for some of the higher lying levels, these ratios are plotted as a function of temperature for electron densities of 10^9, 10^{10}, and 10^{11} cm^{-3} in Figs. 8 and 9.

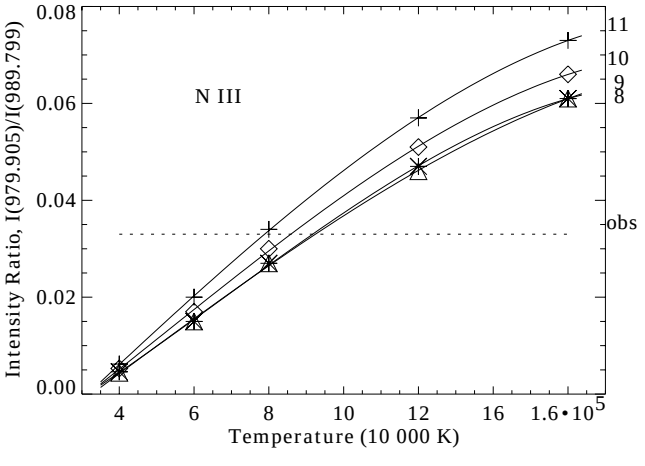

Fig. 8. Plot of the intensity ratio $I(979.92)/I(989.79)$ of N III as a function of temperature, in photon units, for electron densities of 10^9, 10^{10}, and 10^{11} cm^{-3}, indicated by the three solid lines. The observed ratio, 0.033, is shown by the dotted line, and indicates temperatures of about 90 000 K, depending slightly on the assumed density. For comparison, the temperature at which the abundance of the N^{2+} ion is maximized is 80 000 K (Arnaud & Rothenflug 1985)

Proton rates between the fine structure levels of the ground configuration and among the fine structure levels of the $2s2p^2\ ^4P$ term are also included, calculated in a manner similar to that described for dipole transitions in Laming et al. (1996). Agreement between these rates

and the more sophisticated calculations for the ground configurations only of Heil et al. (1982) and Foster et al. (1996) is very good. The temperature inferred from the N III ratio, 8.6 10^4 K, (for a density of 10^{10} cm^{-3}) is just slightly above the temperature of 8 10^4 K where the ion fraction for N^{2+} should be maximal, according to Arnaud & Rothenflug (1985). For O IV, the temperature at the same density is 2.2 10^5 K, rather higher compared to the prediction of 1.6 10^5 K, also from Arnaud & Rothenflug (1985).

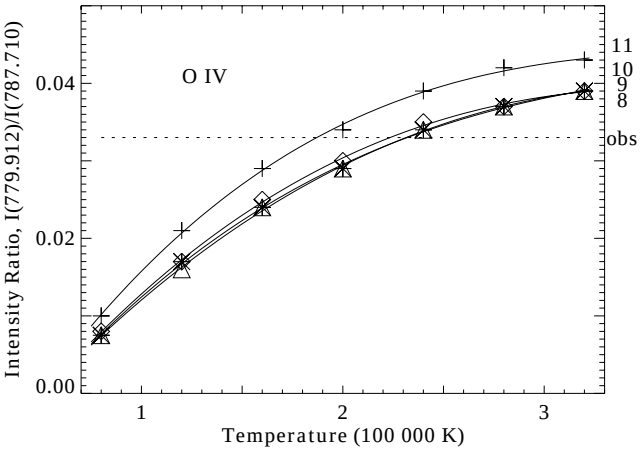

Fig. 9. Plot of the intensity ratio $I(779.91)/I(787.71)$ of O IV as a function of temperature, in photon units, for electron densities of 10^9, 10^{10}, and 10^{11} cm^{-3}, indicated by the three solid lines. The observed ratio, 0.033, is shown by the dotted line, and indicates temperatures of about 200 000 K, depending slightly on the assumed density. For comparison, the temperature at which the abundance of the O^{3+} ion is maximized is 160 000 K (Arnaud & Rothenflug 1985)

A further temperature diagnostic is possible with the ratio

$$I\left(2s2p\ ^1P_1 - 2p^2\ ^1S_0\right)/I\left(2s^2\ ^1S_0 - 2s2p\ ^1P_1\right)$$

in N IV with lines falling at 955.33 and 765.15 Å respectively. Using data from Keenan et al. (1984) the intensity ratio as a function of temperature for densities of 10^9, 10^{10}, and 10^{11} cm^{-3} is plotted in Fig. 10. As in the case with Ne VI, the lines are identified, but difficulties exist with measuring the 955.33 Å line, partially blended as it is with two lines from Fe III.

Temperatures deduced from line intensity ratios higher than those predicted for the particular ion in collisional ionization equilibrium may indicate departures from this equilibrium. This would mean that the plasma, instead of being in a steady state as assumed in the atomic physics statistical equilibrium calculations, is instead transiently ionizing and recombining. One ion that is very sensitive to such changes in temperature is He^+, due to the very high (> 50 eV) excitation thresholds for its emission lines

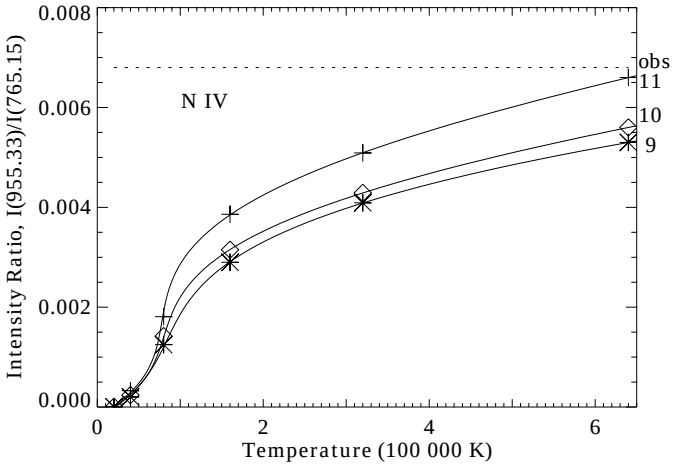

Fig. 10. Plot of the intensity ratio $I(955.33)/I(765.15)$ of N IV as a function of temperature, in photon units, for electron densities of 10^9, 10^{10}, and 10^{11} cm^{-3}, indicated by the three solid lines. Densities below 10^9 are indistinguishable from the 10^9 curve

compared to its usual temperature of formation (Laming & Feldman 1992). In Fig. 11 we plot the intensity ratio of the N III 989.79 line to the He II 992.34 (2s − 7p) line, calculated under a few simple assumptions, to be discussed in more detail below. The two solid curves give the intensity ratio in the limits that the He II 1s − 7p line is completely optically thick, in which case more radiation comes out in the Balmer series, or completely optically thin. An abundance ratio $A(\mathrm{He})/A(\mathrm{N})$ of 870 has been assumed (Grevesse & Anders 1989). The curve illustrates the basic result that only for temperatures considerably in excess of 10^5 K does the intensity ratio predicted by the calculation start to come anywhere near the observed value.

At this stage we should outline the simplifications that have gone into the calculation. Firstly, the fractional ion abundance for each ion has been assumed to be 1. Arnaud & Rothenflug (1985) would predict lower values, but this calculation is not really relevant when considering departures from ionization equilibrium. Hence the ratio has been formed by calculating the emission rate in each ion for the range of temperatures, and by multiplying by the appropriate branching ratio. We have also assumed that only excitations from the ground state of He^+ are important. Proton collisions effectively transfer population in the metastable 2s level to the 2p (Zygelman & Dalgarno 1987), and for the optical depths likely in the He II 1s − 2p transition, insufficient population will be present in the 2p levels to affect the populations of higher lying levels (Laming & Feldman 1992). We have neglected proton collisions among the various levels corresponding to $n = 7$, and have calculated the branching ratio for the Balmer transition in the cases of the optically thick and thin Lyman transition from formulae for

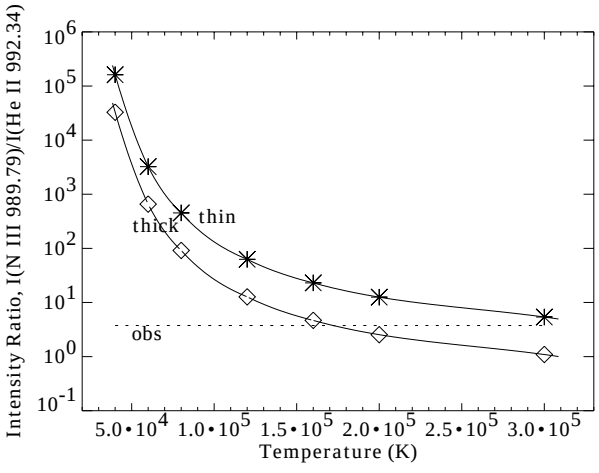

Fig. 11. Plot of the intensity ratio I(N III 989.79)/I(He II 992.34) as a function of temperature, in photon units, for an electron density of 10^{10} cm^{-3}. The two solid lines give the intensity ratio under conditions where the 1s − 7p Lyman line of He^+ is optically thin or thick. The emission rates for each line are weighted by an abundance ratio He/N of 870, but not by the ionization fractions. The observed ratio, 3.76, is shown by the dotted line, and indicates temperatures substantially greater than 100 000 K. For comparison, the temperatures at which the abundance of the He^+ and N^{2+} ions are maximized are 50 000 K and 80 000 K (Arnaud & Rothenflug 1985)

the dipole A-coefficients given in Bethe & Salpeter (1957). It is difficult to obtain accurate electron impact excitation rates for such highly excited levels as $n = 7$. We have taken an approximate collision strength by scaling the collision strengths for 1s − 2p and 1s − 3p excitation of Aggarwal et al. (1992) by the ratios of the absorption oscillator strengths divided by the excitation threshold to get a value of 0.006. While such a procedure is accurate for asymptotically high energies, at lower energies (but still above the ionization threshold) it has been shown (Bray et al. 1993) that continuum wavefunctions must be included in close coupling expansions to get the excitation collision strengths correct. Such calculations are available for excitations between the $n = 1$, 2, 3 levels (Aggarwal et al. 1992) where the effect of the continuum in reducing the excitation collision strengths may easily be seen. Thus it appears that our estimate of the 1s − 7p collision strength may well be an overestimate. For these reasons we have not performed a complete statistical equilibrium calculation for the He II ion, but just given an estimate of the emission rate. We emphasise that the processes we have neglected (excluding cascades) will all act to reduce our predicted He II intensity, making the problem of anomalously high He II line intensities worse.

The fact that in the absence of diffusion effects (see e.g., Fontenla et al. 1993; Hansteen et al. 1994) which we consider to be unlikely, the He II emission can only be understood quantitatively by increasing the temperature at which its emission is assumed to occur implies that the plasma must be transiently ionizing, and that the electron temperature increases on a timescale fast compared to the ionization time, making the plasma underionized. Such a notion is a radical departure from traditional models of the solar transition region (e.g., Vernazza et al. 1981), but is becoming increasingly favoured in the light of recent data.

6. Conclusion

The solar spectrum in the SUMER wavelength range is rich in emission lines. The analysis of this near-limb quiet-Sun spectrum revealed spectral details in the range from 660 Å to 1175 Å and resulted in a line list, including very faint lines. Only few lines remained unidentified. Other spectra from different regions of the Sun have to be analysed to find out commonality and variability of spectral features of the Sun.

Acknowledgements. The SUMER project is financially supported by DARA, CNES, NASA and PRODEX (Swiss contribution). Additional financial support is being provided by the participating institutions along with general administrative assistance at various phases of the project. The instrument development and/or commissioning has been carried out by a large dedicated team of engineers, scientists, and technicians co-ordinated by a management support group, and scientific advice was provided by a large group of Associate Scientists.

The authors greatly acknowledge their contributions. We particularly appreciate the efforts of the SUMER operations team.

References

Aggarwal K.M., Callaway J., Kingston A.E., Unnikrishnan K., 1992, ApJS 80, 473
Arnaud M., Rothenflug R., 1985, A&AS 60, 425
Bartoe J.-D.F., Brueckner G.E., Purcell J.D., Tousey R., 1977, Appl. Opt. 16, 879
Bethe H.A., Salpeter E.E., 1957, in: The Quantum Mechanics of One and Two Electron Atoms. New York: Plenum
Bray I., McCarthy I.E., Wigley J., Stelbovics A.T., 1993, J. Phys. B 26, L831
Brekke P., Kjeldseth-Moe O., Bartoe J.-D.F., Brueckner G.E., 1991, ApJS 75, 1337
Burton W.M., Ridgeley A., 1970, Solar Phys. 14, 3
Cohen L., Feldman U., Doscheck G.A., 1978, ApJS 37, 393
Dankwort W., Trefftz E., 1978, A&A 65, 93
Edlén B., 1983, Phys. Scripta 28, 483
Feldman U., 1995, Comments At. Mol. Phys. 31, 11
Feldman U., Doschek G.A., Seely J.S., 1988, J. Opt. Soc. Am. 5, 2237
Feldman U., Doschek G.A., 1991, ApJS 75, 925
Fontenla J.M., Avrett E.H., Loeser R., 1993, ApJ 406, 319
Foster V.J., Keenan F.P., Reid R.H.G., 1996, A&A 308, 1009
Grevesse N., Anders E., 1989, in: Cosmic Abundances of Matter, AIP Conf. Proc. 183, Waddington C.J. (ed.) New York: AIP, p. 1

Hansteen V.H., Leer E., Holzer T.E., 1994, ApJ 428, 843
Heil T.G., Green S., Dalgarno A., 1982, Phys. Rev. A 26, 3293
Hollandt J., Schühle U., Paustian W., Curdt W., Kühne M., Wende B., Wilhelm K., 1996, Appl. Opt. 35, 5125
Keenan F.P., Berrington K.A., Burke P.G., Kingston A.E., Dufton P.L., 1984, MNRAS 207, 459
Keenan F.P., Foster V.J., Reid R.H.G., Doyle J.G., Zhang H.L., Pradhan A.K., 1995, A&A 300, 534
Kelly R.L., 1987, J. Phys. Chem. Ref. Data 16, 1
Laming J.M., Feldman U., 1992, ApJ 386, 364
Laming J.M., Raymond J.C., McLaughlin B.M., Blair W.P., 1996, ApJ 472, 267
Lemaire P., Wilhelm K., Curdt W., et al., 1997, Solar Phys. 170, 105
Noyes R.W., Raymond J.C., Doyle J.G., Kingston A.E., 1985, ApJ 297, 805
Nussbaumer H., Storey P.J., 1979, A&A 71, L5
Nussbaumer H., Storey P.J., 1982, A&A 115, 205
Sandlin G.D., Bartoe J.-D.F., Brueckner G.E., Tousey R., VanHoosier M.E., 1986, ApJS 61, 801
Siegmund O.H.W., Gummin M.A., Stock J.M., Marsh D., Raffanti T., Sasseen T., Tom J., Welsh B., Gaines G.A., Jelinsky P., Hull J., 1994, Proc. SPIE 2280, 89
Stafford R.P., Bell K.L., Hibbert A., 1994, MNRAS 266, 715
Vernazza J.E., Reeves E.M., 1978, ApJS 37, 485
Vernazza J.E., Avrett E.H., Loeser R., 1981, ApJS 45, 635
Wilhelm K., Curdt W., Marsch E., et al., 1995, Solar Phys. 162, 189
Wilhelm K., Lemaire P., Curdt W., et al., 1997a, Solar Phys. 170, 75
Wilhelm K., Lemaire P., Feldman U., Hollandt J., Schühle U., Curdt W., 1997b, Appl. Opt. 36, No. 25
Zhang H.L., Graziani M., Pradhan A.K., 1994, A&A 283, 319
Zygelman B., Dalgarno A., 1987, Phys. Rev. A 35, 4085

Table 1. Line List – This list of spectral lines in the 660 – 1175 Å wavelength range including some 2nd order lines below 590 Å was compiled from a spectrum which was recorded with detector B on the solar disk near the north limb. It was generated from a number of sections recorded on the KBr photocathode each about 20 Å wide, and complemented by bare photocathode lines at the lower wavelength limit

Peak[1], mW sr^{-1}m^{-2}Å^{-1}	λ_{lit}, Å[2]	λ_{obs}, Å[3]	Line	Transition	Remarks
–	657.34	657.34	S IV	$3s^23p\ ^2P_{1/2}$ – $3s^23d\ ^2D_{3/2}$	on attenuator
142	661.42	661.42*	S IV	$3s^23p\ ^2P_{3/2}$ – $3s^23d\ ^2D_{5/2}$	on bare
33	663.16	663.16	S V	$3s3p\ ^3P_2$ – $3s3d\ ^3D_3$	on bare
5	671.016	671.02	N II	$2s^22p^2\ ^3P_1$ – $2s^22p3s\ ^3P_2$	
	671.386		N II	$2s^22p^2\ ^3P_2$ – $2s^22p3s\ ^3P_2$	
15	671.411	671.41	N II	$2s^22p^2\ ^3P_0$ – $2s^22p3s\ ^3P_1$	
	671.630		N II	$2s^22p^2\ ^3P_1$ – $2s^22p38\ ^3P_1$	
5	671.773	671.75	N II	$2s^22p^2\ ^3P_1$ – $2s^22p3s\ ^3P_0$	
4	672.001	672.00*	N II	$2s^22p^2\ ^3P_2$ – $2s^22p3s\ ^3P_1$	
10	672.948	672.98	O II	$2s^22p^3\ ^2P_{3/2}$ – $2s^22p^23s\ ^2P_{3/2}$	
7	673.768	673.80	O II	$2s^22p^3\ ^2P_{1/2}$ – $2s^22p^23s\ ^2P_{1/2}$	
10	677.75	677.74	S III	$3s^23p^2\ ^3P_0$ – $3s^23p3d\ ^3D_1$	
18	678.46	678.46*	S III	$3s^23p^2\ ^3P_1$ – $3s^23p3d\ ^3D_2$	
9	679.11	679.14	S III	$3s^23p^2\ ^3P_1$ – $3s^23p3d\ ^3D_1$	
39	680.69	680.70	S III	$3s^23p^2\ ^3P_2$ – $3s^23p3d\ ^3D_3$	
20	680.95	680.97	S III	$3s^23p^2\ ^3P_2$ – $3s^23p3d\ ^3D_2$	
6	681.50	681.51	S III	$3s^23p^2\ ^3P_0$ – $3s^23p4s\ ^3P_1$	
9	681.72	681.66	Na IX	$2s\ ^2S_{1/2}$ – $2p\ ^2P_{3/2}$	
5	683.07	683.05	S III	$3s^23p^2\ ^3P_1$ – $3s^23p4s\ ^3P_0$	
21	683.47	683.53	S III	$3s^23p^2\ ^3P_2$ – $3s^23p4s\ ^3P_2$	
		684.71	?		
45	684.996	684.99*	N III	$2s^22p^2\ ^2P_{1/2}$ – $2s^22p^2\ ^2P_{3/2}$	
93	685.513	685.50	N III	$2s^22p^2\ ^2P_{1/2}$ – $2s^22p^2\ ^2P_{1/2}$	
204	685.816	685.78	N III	$2s^22p^2\ ^2P_{3/2}$ – $2s^22p^2\ ^2P_{3/2}$	
48	686.335	686.32	N III	$2s^22p^2\ ^2P_{3/2}$ – $2s^22p^2\ ^2P_{1/2}$	
		686.77	?		
20	687.0526	687.05	C II	$2s^22p\ ^2P_{1/2}$ – $2s^23d\ ^2D_{3/2}$	
30	687.3453	687.34	C II	$2s^22p\ ^2P_{3/2}$ – $2s^23d\ ^2D_{5/2}$	
	687.3521		C II	$2s^22p\ ^2P_{3/2}$ – $2s^23d\ ^2D_{3/2}$	
4		688.90	?		
4		690.09	?		
30	690.526	690.53	C III	$2s2p\ ^1P_1$ – $2s3s\ ^1S_0$	
6	691.187	691.21	N III	$2s2p^2\ ^2D_{5/2}$ – $2s^23p\ ^2P_{3/2}$	?
6	691.388	691.38	N III	$2s2p^2\ ^2D_{3/2}$ – $2s^23p\ ^2P_{1/2}$	?
6	694.14	694.07	Na IX	$2s\ ^2S_{1/2}$ – $2p\ ^2P_{1/2}$	
5	694.71	694.72	S II	$3s^23p^3\ ^2D_{5/2}$ – $3s^23p^24d\ ^2D_{5/2}$	?
16	696.612	696.62	S V	$3s3p\ ^1P_1$ – $3s3d\ ^1D_2$	
		696.81	?		
		697.16	?		
6		698.72	S III	$3s^23p^2\ ^3P_0$ – $3s^23p3d\ ^3P_1$	
8	698.73	698.72	S III	$3s^23p^2\ ^3P_1$ – $3s^23p3d\ ^3P_2$	
	700.15	700.11	S III		
28	700.245	700.24	Ar VIII	$3s\ ^2S_{1/2}$ – $3p\ ^2P_{3/2}$	
	700.29		S III	$3s^23p^2\ ^3P_1$ – $3s^23p3d\ ^3P_0$	
137	702.332	702.31*	O III	$2s^22p^2\ ^3P_0$ – $2s^22p^3\ ^3P_1$	
319	702.822	702.81	O III	$2s^22p^2\ ^3P_1$ – $2s2p^3\ ^3P_0$	
	702.899		O III	$2s^22p^2\ ^3P_1$ – $2s2p^3\ ^3P_2$	
500	703.850	703.81	O III	$2s^22p^2\ ^3P_2$ – $2s2p^3\ ^3P_2$	
16	705.72	706.02	Mg IX	$1s^22s^2\ ^1S_0$ – $1s^22s2p\ ^3P_1$	?
9	706.48	706.47	S VI	$3p\ ^2P_{1/2}$ – $3d\ ^2D_{3/2}$	
105	780.324	780.32	Ne VIII	$2s\ ^2S_{1/2}$ – $2p\ ^2P_{1/2}$	
9		781.65	?		
11	761.128	761.15	O V	$2s2p\ ^3P_1$ – $2p^2\ ^3P_1$	
46	762.003	762.00*	O V	$2s2p\ ^3P_2$ – $2p^2\ ^3P_1$	
26	763.340	763.31	N III	$2s^22p\ ^2P_{1/2}$ – $2s2p^2\ ^2S_{1/2}$	
49	764.357	764.36	N III	$2s^22p\ ^2P_{3/2}$ – $2s2p^2\ ^2S_{1/2}$	
515	765.148	765.15**	N IV	$2s^2\ ^1S_0$ – $2s2p\ ^1P_1$	
7	767.06	767.07	Ar VI	$3s^23p\ ^2P_{3/2}$ – $3s3p^2\ ^2D_{5/2}$	?
177	770.409	770.41*	Ne VIII	$2s\ ^2S_{1/2}$ – $2p\ ^2P_{3/2}$	
7	771.544	771.4	N III	$2s2p^2\ ^4P_{1/2}$ – $2p^3\ ^4S_{3/2}$	
7	771.901	771.9	N III	$2s2p^2\ ^4P_{3/2}$ – $2p^3\ ^4S_{3/2}$	
13	772.385	772.25	N III	$2s2p^2\ ^4P_{5/2}$ – $2p^3\ ^4S_{3/2}$	
7	772.891	772.85	N III	$2s2p^2\ ^2D_{5/2}$ – $2p^3\ ^2P_{3/2}$	
	772.955		N III	$2s2p^2\ ^2D_{3/2}$ – $2s2p^2\ ^2P_{1/2}$	
15	774.518	774.47	O V	$2s2p\ ^1P_1$ – $2p^2\ ^1S_0$	
8		775.34	?		
19	775.965	775.95	N II	$2s^22p^2\ ^1D_2$ – $2s2p^2\ ^1D_2$	
11		777.91	?		
	779.734		O IV	$2s2p^2\ ^2D_{5/2}$ – $2p^3\ ^2D_{3/2}$	
	779.821		O IV	$2s2p^2\ ^2D_{3/2}$ – $2p^3\ ^2D_{3/2}$	
20	779.912	779.88	O IV	$2s2p^2\ ^2D_{5/2}$ – $2p^3\ ^2D_{5/2}$	
	779.997		O IV	$2s2p^2\ ^2D_{3/2}$ – $2p^3\ ^2D_{5/2}$	

Table 1. continued

Peak[1], mW sr^{-1}m^{-2}Å^{-1}	λ_{lit}, Å[2]	λ_{obs}, Å[3]	Line	Transition			Remarks
8	782.36	782.29	Mg VIII	$2s^22p\ ^2P_{3/2}$	–	$2s2p^2\ ^4P_{3/2}$	
266	786.48	786.47	S V	$3s^2\ ^1S_0$	–	$3s3p\ ^1P_1$	
470	787.711	787.72	O IV	$2s^22p\ ^2P_{1/2}$	–	$2s2p^2\ ^2D_{3/2}$	
	790.109		O IV	$2s^22p\ ^2P_{3/2}$	–	$2s2p^2\ ^2D_{3/2}$	]
896	790.199	790.19	O IV	$2s^22p\ ^2P_{3/2}$	–	$2s2p^2\ ^2D_{5/2}$	]
	796.638		O II	$2s^22p^3\ ^2P_{1/2}$	–	$2s2p^4\ ^2D_{3/2}$	]
26	796.661	796.66	O II	$2s^22p^3\ ^2P_{3/2}$	–	$2s2p^4\ ^2D_{5/2}$	]
	806.384	806.31	C II	$2s2p^2\ ^4P_{3/2}$	–	$2s2p3s\ ^4P_{5/2}$	]
	806.533		C II	$2s2p^2\ ^4P_{1/2}$	–	$2s2p3s\ ^4P_{3/2}$	]
20	806.568	806.57	C II	$2s2p^2\ ^4P_{5/2}$	–	$2s2p3s\ ^4P_{5/2}$	]
	806.676		C II	$2s2p^2\ ^4P_{3/2}$	–	$2s2p3s\ ^4P_{3/2}$	]
	806.686		C II	$2s2p^2\ ^4P_{1/2}$	–	$2s2p3s\ ^4P_{1/2}$	]
14	806.830	806.82	C II	$2s2p^2\ ^4P_{3/2}$	–	$2s2p3s\ ^4P_{1/2}$	]
	806.860		C II	$2s2p^2\ ^4P_{5/2}$	–	$2s2p3s\ ^4P_{3/2}$	]
		809.6	?				]
24	809.668	809.67*	S IV	$3s^23p\ ^2P_{1/2}$	–	$3s3p^2\ ^2S_{1/2}$	]
17	815.049	815.05	Si IV	$3p\ ^2P_{1/2}$	–	$4s\ ^2S_{1/2}$	
28	815.952	815.95	S IV	$3s^23p\ ^2P_{3/2}$	–	$3s3p^2\ ^2S_{1/2}$	
26	818.129	818.13	Si IV	$3p\ ^2P_{3/2}$	–	$4s\ ^2S_{1/2}$	
19		820.86	?				
26		822.56	?				
	832.762		O II	$2s^22p^3\ ^4S_{3/2}$	–	$2s2p^4\ ^4P_{1/2}$	]
216	832.927	832.92	O III	$2s^22p^2\ ^3P_0$	–	$2s2p^3\ ^3D_1$	]
192	833.332	833.33	O II	$2s^22p^3\ ^4S_{3/2}$	–	$2s2p^4\ ^4P_{3/2}$	
551	833.742	833.76*	O III	$2s^22p^2\ ^3P_1$	–	$2s2p^3\ ^3D_2$	
259	834.462	834.45	O II	$2s^22p^3\ ^4S_{3/2}$	–	$2s2p^4\ ^4P_{5/2}$	
	835.096		O III	$2s^22p^2\ ^3P_2$	–	$2s2p^3\ ^3D_2$	]
842	835.292	835.26	O III	$2s^22p^2\ ^3P_2$	–	$2s2p^3\ ^3D_3$	]
37	854.87	854.87	S V	$3s3p\ ^3P_2$	–	$3p^2\ ^3P_2$	?
49	858.0918	858.10	C II	$2s^22p\ ^2P_{1/2}$	–	$2s^23s\ ^2S_{1/2}$	
67	858.5590	858.55*	C II	$2s^22p\ ^2P_{3/2}$	–	$2s^23s\ ^2S_{1/2}$	
53	859.626	859.68	Fe III	$3d^6\ ^5D_2$	–	$3d^5(a^4G)4p\ ^5D_3$	]
	859.721		Fe III	$3d^6\ ^5D_4$	–	$3d^5(a^4G)4p\ ^5F_5$	]
43	861.761	861.75	Fe III	$3d^6\ ^5D_1$	–	$3d^5(a^2G)4p\ ^5F_2$	]
	861.832		Fe III	$3d^6\ ^5D_3$	–	$3d^5(a^4G)4p\ ^5F_4$	]
40	864.034	863.90	Fe III	$3d^6\ ^5D_2$	–	$3d^5(a^4P)4p\ ^5F_3$	
64	895.18	895.10	Ne VII	$2s^2\ ^1S_0$	–	$2s2p\ ^3P_1$	
111	903.6235	903.63*	C II	$2s^22p\ ^2P_{1/2}$	–	$2s2p^2\ ^2P_{3/2}$	
139	903.9616	904.01	C II	$2s^22p\ ^2P_{1/2}$	–	$2s2p^2\ ^2P_{1/2}$	]
188	904.1416	904.15	C II	$2s^22p\ ^2P_{3/2}$	–	$2s2p^2\ ^2P_{3/2}$	]
95	904.4801	904.48	C II	$2s^22p\ ^2P_{3/2}$	–	$2s2p^2\ ^2P_{1/2}$	
	914.576		H I	$1s\ ^2S$	–	$18p\ ^2P$	not resolved
	914.919		H I	$1s\ ^2S$	–	$17p\ ^2P$	not resolved
	915.329		H I	$1s\ ^2S$	–	$16p\ ^2P$	not resolved
82	915.612	915.59	N II	$2s^22p^2\ ^3P_0$	–	$2s2p^3\ ^3P_1$	
	915.824		H I	$1s\ ^2S$	–	$15p\ ^2P$	not resolved
	915.962		N II	$2s^22p^2\ ^3P_1$	–	$2s2p^3\ ^3P_0$	]
100	916.012	916.00	N II	$2s^22p^2\ ^3P_1$	–	$2s2p^3\ ^3P_2$	]
	916.429		H I	$1s\ ^2S$	–	$14p\ ^2P$	not resolved
122	916.701	916.69 *	N II	$2s^22p^2\ ^3P_2$	–	$2s2p^3\ ^3P_2$	
(44)	917.181		H I	$1s\ ^2S$	–	$13p\ ^2P$	self-absorption
(51)	918.129		H I	$1s\ ^2S$	–	$12p\ ^2P$	self-absorption
14	918.724	918.73	O I	$2s^22p^4\ ^3P_0$	–	$2s^22p^312d\ ^3D_1$	
(49)	919.351		H I	$1s\ ^2S$	–	$11p\ ^2P$	] self-absorption
26	919.658	919.69	O I	$2s^22p^4\ ^3P_2$	–	$2s^22p^310d\ ^3D_3$	]
13	919.908	919.91	O I	$2s^22p^4\ ^3P_2$	–	$2s^22p^311s\ ^3S_1$	]
	919.971	919.97	O I	$2s^22p^4\ ^3P_0$	–	$2s^22p^311d\ ^3D_1$	]
(50)	920.963		H I	$1s\ ^2S$	–	$10p\ ^2P$	self-absorption
39		921.7	O I ?				
62	921.992	922.01	N IV	$2s2p\ ^3P_1$	–	$2p^2\ ^3P_2$	
39	922.519	922.51	N IV	$2s2p\ ^3P_0$	–	$2p^2\ ^3P_1$	
	923.057		N IV	$2s2p\ ^3P_1$	–	$2p^2\ ^3P_1$	]
(87)	923.150		H I	$1s\ ^2S$	–	$9p\ ^2P$	] self-absorption
	923.220		N IV	$2s2p\ ^3P_2$	–	$2p^2\ ^3P_2$	]
29	923.675	923.60	N IV	$2s2p\ ^3P_1$	–	$2p^2\ ^3P_0$	
46	924.283	924.27	N IV	$2s2p\ ^3P_2$	–	$2p^2\ ^3P_1$	
25	924.952	924.97*	O I	$2s^22p^4\ ^3P_2$	–	$2s^22p^38d\ ^3D_3$	
13	925.442	925.45	O I	$2s^22p^4\ ^3P_2$	–	$2s^22p^39s\ ^3S_1$	
(66)	926.226		H I	$1s\ ^2S$	–	$8p\ ^2P$	] self-absorption
	926.295	926.33	O I	$2s^22p^4\ ^3P_1$	–	$2s^22p^38d\ ^3D_2$	]
	926.809		O I	$2s^22p^4\ ^3P_1$	–	$2s^22p^39s\ ^3S_1$	]
14	926.903	926.91	O I	$2s^22p^4\ ^3P_0$	–	$2s^22p^38d\ ^3D_1$	]
8	927.178	927.22	Fe II	$3d^6(a^5D)4s\ ^6D_{7/2}$	–	$24^\circ\ _{7/2}$	?
6	927.394	927.41	O I	$2s^22p^4\ ^3P_0$	–	$2s^22p^39s\ ^3S_1$	
8	–	927.89	He II	$2s\ ^2S$	–	$15p\ ^2P$	]
				$2p\ ^2P$	–	$15d\ ^2D$	]
6	928.004	928.06	Fe III	$3d^6\ ^1F_3$	–	$3d^5(b^2F)4p\ ^1F_3$	
11	928.474	928.50	Fe III	$3d^6\ ^3G_5$	–	$3d^5(a^2I)4p\ ^3H_6$	
10	929.163	929.22	Fe III	$3d^6\ ^3G_4$	–	$3d^5(a^2I)4p\ ^3H_5$	
31	929.5168	929.56	O I	$2s^22p^4\ ^3P_2$	–	$2s^22p^37d\ ^3D_3$	
	930.086		Fe III	$3d^6\ ^3G_3$	–	$3d^5(a^2I)4p\ ^3H_4$	]
20	930.2566	930.33	O I	$2s^22p^4\ ^3P_2$	–	$2s^22p^38s\ ^3S_1$	]
(82)	930.748		H I	$1s\ ^2S$	–	$7p\ ^2P$	] self-absorption
	930.8862		O I	$2s^22p^4\ ^3P_1$	–	$2s^22p^37d\ ^3D_2$	]
18	931.4820	931.50	O I	$2s^22p^4\ ^3P_0$	–	$2s^22p^37d\ ^3D_1$	
13	931.6282	931.64	O I	$2s^22p^4\ ^3P_1$	–	$2s^22p^38s\ ^3S_1$	
4	932.0537	932.08	Ar II	$2s^22p^5\ ^2P_{1/2}$	–	$2s2p^6\ ^2S_{1/2}$	
7	932.2249	932.23	O I	$2s^22p^4\ ^3P_0$	–	$2s^22p^38s\ ^3S_1$	
235	933.38	933.39	S VI	$3s\ ^2S_{1/2}$	–	$3p\ ^2P_{3/2}$	
10	934.703	934.69	Fe III	$3d^6\ ^3P_2$	–	$3d^5(a^4P)4p\ ^3S_1$	
12	935.1930	935.19*	O I	$2s^22p^4\ ^1D_2$	–	$2s^22p^34s\ ^1D_2$	
32	936.6295	936.62	O I	$2s^22p^4\ ^3P_2$	–	$2s^22p^36d\ ^3D_3$	
(97)	937.803		H I	$1s\ ^2S$	–	$6p\ ^2P$	] self-absorption
	937.8405		O I	$2s^22p^4\ ^3P_2$	–	$2s^22p^37s\ ^3S_1$	]
	938.0200		O I	$2s^22p^4\ ^3P_1$	–	$2s^22p^36d\ ^3D_2$	]
21	938.6249	938.62*	O I	$2s^22p^4\ ^3P_0$	–	$2s^22p^36d\ ^3D_1$	
14	939.2346	939.27	O I	$2s^22p^4\ ^3P_1$	–	$2s^22p^37s\ ^3S_1$	
9	939.8412	939.86	O I	$2s^22p^4\ ^3P_0$	–	$2s^22p^37s\ ^3S_1$	
8		941.53	?				
15	942.363	942.39	Fe III	$3d^6\ ^1F_3$	–	$3d^5(a^2H)4p\ ^1G_4$	]
	942.490		He II	$2s\ ^2S_{1/2}$	–	$11p\ ^2P_{3/2}$	]
	942.538	942.56	**He II**	$2p\ ^2P_{3/2}$	–	$11d\ ^2D_{5/2}$	]
8		943.07	C III ?				
7		943.89	?				
15		944.34	Si VIII ?				]
120	944.54	944.52	S VI	$3s\ ^2S_{1/2}$	–	$3p\ ^2P_{1/2}$	]

Table 1. continued

Peak[1], mW sr^{-1}m^{-2}Å^{-1}	λ_{lit}, Å[2]	λ_{obs}, Å[3]	Line	Transition			Remarks
	945.191		C I	$2s^22p^2\ ^3P_0$	–	$2s2p^3\ ^3S_1$	]
6	945.338	945.32	C I	$2s^22p^2\ ^3P_1$	–	$2s2p^3\ ^3S_1$	]
6	945.579	945.61	C I	$2s^22p^2\ ^3P_2$	–	$2s2p^3\ ^3S_1$	]
	945.977	945.99	C II	$2s2p^2\ ^2S_{1/2}$	–	$2s2p3d^2P_{1/2}$	]
8	946.198	946.14	C II	$2s2p^2\ ^2S_{1/2}$	–	$2s2p3d\ ^2P_{3/2}$	]
7	946.7032	946.67	Mg II	$3s\ ^2S_{1/2}$	–	$6p\ ^2P_{3/2}$	?
9	948.322	948.36	Fe III	$3d^6\ ^3P_2$	–	$3d^5(a^4D)4p\ ^3D_3$	
33	948.6855	948.69*	O I	$2s^22p^4\ ^3P_2$	–	$2s^22p^35d\ ^3D_3$	
(168)	949.743		H I	$1s\ ^2S$	–	$5p\ ^2P$	]
	950.1121		O I	$2s^22p^4\ ^3P_1$	–	$2s^22p^35d\ ^3D_2$	] self-absorption
33	950.334	950.36	Fe III	$3d^6\ ^1I_6$	–	$3d^5(a^4F)4p\ ^5G_6$	
52	950.722	950.72	Fe III	$3d^6\ ^3P_0$	–	$3d^5(a^4P)4p\ ^3S_1$	]
	950.7327		O I	$2s^22p^4\ ^3P_0$	–	$2s^22p^35d\ ^3D_1$	]
	950.8846		O I	$2s^22p^4\ ^3P_2$	–	$2s^22p^36s\ ^3S_1$	]
4		951.66	?				
11	952.3178	952.32*	O I	$2s^22p^4\ ^3P_1$	–	$2s^22p^36s\ ^3S_1$	
9	952.9413	952.95	O I	$2s^22p^4\ ^3P_0$	–	$2s^22p^36s\ ^3S_1$	
6	953.4150	953.39	N I	$2s^22p^3\ ^4S_{3/2}$	–	$2s^22p^23d\ ^4P_{1/2}$	]
6	953.6548	953.64	N I	$2s^22p^3\ ^4S_{3/2}$	–	$2s^22p^23d\ ^4P_{3/2}$	]
5	953.9698	953.99	N I	$2s^22p^3\ ^4S_{3/2}$	–	$2s^22p^23d\ ^4P_{5/2}$	]
4	955.141	955.13	Fe III	$3d^6\ ^3D_3$	–	$3d^5(a^2F)4p\ ^3G_4$	]
8	955.335	955.33	N IV	$2s2p\ ^1P_1$	–	$2p^2\ ^1S_0$	]
7	955.572	955.57	Fe III	$3d^6\ ^1D_2$	–	$3d^5(a^2F)4p\ ^1F_3$	]
4	957.88		S II	$3s^23p^3\ ^2D_{3/2}$	–	$3s^23p^23d\ ^2D_{3/2}$	
	958.675		He II	$2s\ ^2S_{1/2}$	–	$9p\ ^2P_{3/2}$	]
21	958.724	958.70	He II	$2p\ ^2P_{3/2}$	–	$9d\ ^2D_{5/2}$	]
9	959.552	959.57	Fe III	$3d^6\ ^3P_1$	–	$3d^5(a^4D)4p\ ^3D_2$	
8	961.901	961.90	Fe III	$3d^6\ ^1D_2$	–	$3d^5(a^2F)4p\ ^1D_2$	
8		962.44	?				]
6	962.655	962.67	Fe III	$3d^6\ ^1S_0$	–	$3d^5(a^2D)4p\ ^1P_1$	]
8	963.9904	964.00	N I	$2s^22p^3\ ^4S_{3/2}$	–	$2s^22p^24s\ ^4P_{5/2}$	
7	964.6258	964.64	N I	$2s^22p^3\ ^4S_{3/2}$	–	$2s^22p^24s\ ^4P_{3/2}$	
6	965.0415	965.08	N I	$2s^22p^3\ ^4S_{3/2}$	–	$2s^22p^24s\ ^4P_{1/2}$	
17	967.197	967.20*	Fe III	$3d^6\ ^3F_4$	–	$3d^5(a^4D)4p\ ^3D_3$	
11	968.955	968.95	Fe III	$3d^6\ ^3F_3$	–	$3d^5(a^4D)4p\ ^3D_2$	
9	969.954	970.00	Fe III	$3d^6\ ^3F_2$	–	$3d^5(a^4D)4p\ ^3D_1$	
29		971.48	?				
44	971.7381	971.74	O I	$2s^22p^4\ ^3P_2$	–	$2s^22p^34d\ ^3D_3$	
(299)	972.537		H I	$1s\ ^2S$	–	$4p\ ^2P$	self-absorption
41	973.2343	973.25	O I	$2s^22p^4\ ^3P_1$	–	$2s^22p^34d\ ^3D_2$	
31	973.8852	973.89	O I	$2s^22p^4\ ^3P_0$	–	$2s^22p^34d\ ^3D_1$	
26	976.4481	976.45	O I	$2s^22p^4\ ^3P_2$	–	$2s^22p^35s\ ^3S_1$	]
6648	977.020	977.04	C III	$2s^2\ ^1S_0$	–	$2s2p\ ^1P_1$	]
22	977.9594	977.96	O I	$2s^22p^4\ ^3P_1$	–	$2s^22p^35s\ ^3S_1$	
17	978.6170	978.62	O I	$2s^22p^4\ ^3P_0$	–	$2s^22p^35s\ ^3S_1$	
11	979.032	979.04	Fe III	$3d^6\ ^1F_3$	–	$3d^5(a^2G)4p\ ^1F_3$	
	979.842		N III	$2s2p^2\ ^2D_{3/2}$	–	$2p^3\ ^2D_{3/2}$	]
14	979.919	979.86	N III	$2s2p^2\ ^2D_{5/2}$	–	$2p^3\ ^2D_{5/2}$	]
50	981.373	981.37*	Fe III	$3d^5(a^4P)4s\ ^5P_2$	–	$3d^5(a^6S)5p\ ^5P_2$	
50	983.860	983.89	Fe III	$3d^6\ ^3H_5$	–	$3d^5(a^4G)4p\ ^3G_4$	
38	985.824	985.82	Fe III	$3d^6\ ^3H_4$	–	$3d^5(a^4G)4p\ ^3G_3$	
12	986.514	986.60	Fe III	$3d^6\ ^3F_4$	–	$3d^5(a^4D)4p\ ^5D_3$	]
	986.637		Fe III	$3d^6\ ^1I_6$	–	$3d^5(a^2I)4p\ ^1H_5$	]
7	988.148	988.15	Fe III	$3d^6\ ^3F_3$	–	$3d^5(a^4P)4p\ ^3D_2$	
48		988.60	?				]
70	988.7734	988.78	O I	$2s^22p^4\ ^3P_2$	–	$2s^22p^33s\ ^3D_3$	]
343	989.790	989.81	N III	$2s^22p\ ^2P_{1/2}$	–	$2s2p^2\ ^2D_{3/2}$	]
	990.1269		O I	$2s^22p^4\ ^3P_1$	–	$2s^22p^33s\ ^3D_1$	]
49	990.2043	990.17	O I	$2s^22p^4\ ^3P_1$	–	$2s^22p^33s\ ^3D_2$	]
42	990.8010	990.79*	O I	$2s^22p^4\ ^3P_0$	–	$2s^22p^33s\ ^3D_1$	]
55	991.232	991.21	Fe III	$3d^6\ ^3F_4$	–	$3d^5(a^4P)4p\ ^3D_3$	
	991.514		N III	$2s^22p\ ^2P_{3/2}$	–	$2s2p^2\ ^2D_{3/2}$	]
779	991.579	991.56	N III	$2s^22p\ ^2P_{3/2}$	–	$2s2p^2\ ^2D_{5/2}$	]
41	992.338	992.36	He II	$2s\ ^2S_{1/2}$	–	$7p\ ^2P_{3/2}$	
28	992.6826	992.68	Si II	$3s^23p\ ^2P_{3/2}$	–	$3s^24d\ ^2D_{5/2}$	
25	993.080	993.08 *	Fe III	$3d^6\ ^3G_4$	–	$3d^5(a^4D)4p\ ^3F_3$	
15	993.519	993.52	Si III	$3s3p\ ^3P_0$	–	$3s4s\ ^3S_1$	
27	994.257	994.22	Fe III	$3d^6\ ^3P_2$	–	$3d^5(a^4P)4p\ ^3P_1$	
37	994.724	994.72	Fe III	$3d^6\ ^3G_3$	–	$3d^5(a^4D)4p\ ^3F_2$	
19	995.150	995.14	Fe III	$3d^6\ ^3F_4$	–	$3d^5(a^4G)4p\ ^3G_5$	]
	995.223		Fe III	$3d^6\ ^3F_4$	–	$3d^5(a^4G)4p\ ^3G_4$	]
30	996.00	996.00*	S II	$3s^23p^3\ ^2D_{5/2}$	–	$3s^23p^23d^2F_{7/2}$	
28	997.081	997.08	Fe III	$3d^6\ ^3P_2$	–	$3d^5(a^4P)4p\ ^3P_2$	]
	997.03 P		Ne VI	$2s^22p\ ^2P_{1/2}$	–	$2s2p^2\ ^2P_{1/2}$	] new wavelength
38	997.389	997.35	Si III	$3s3p\ ^3P_2$	–	$3s4s\ ^3S_1$	]
21	997.599	997.52	Fe III	$3d^6\ ^3F_3$	–	$3d^5(a^4G)4p\ ^3G_4$	] ?
21	999.18 P	999.2	Ne VI	$2s^22p\ ^2P_{3/2}$	–	$2s2p^2\ ^4P_{5/2}$	] new wavelength
	999.376		Fe III	$3d^6\ ^3F_2$	–	$3d^5(a^4G)4p\ ^3G_3$	]
61	999.4974	999.49	O I	$2s^22p^4\ ^1D_2$	–	$2s^22p^33s\ ^1P_1$	]
23	1000.16	1000.18	Ar VI	$3s^23p\ ^2P_{3/2}$	–	$3s3p^24P_{5/2}$	
24	1000.48	1000.50	S II	$3s^23p^3\ ^2D_{3/2}$	–	$3s^23p^23d\ ^2F_{5/2}$	
9	1000.75	1000.85	S II	$3s^23p^3\ ^2D_{5/2}$	–	$3s^23p^23d\ ^2F_{5/2}$	
12	1005.106	1005.10*	Fe III	$3d^5(a^4S)4p^7P_3$	–	$3d^5(a^4G)5s\ ^5G_4$	
17	1005.69 P	1005.78	Ne VI	$2s^22p\ ^2P_{3/2}$	–	$2s2p^2\ ^4P_{3/2}$	new wavelength
29	1006.15	1006.14	S II	$3s^23p^3\ ^2D_{5/2}$	–	$3s^23p^23d\ ^4D_{7/2}$	]
22	1006.341		Fe III	$3d^61G_4$	–	$3d^5(a^7I)4p\ ^3I_5$	]
12	1006.95	1006.89	S II	$3s^23p^3\ ^2D_{3/2}$	–	$3s^23p^23d\ ^4D_{1/2}$	]
13	1007.113	1007.06	Fe III	$3d^63P_1$	–	$3d^5(a^4P)4p\ ^3P_1$	]
27		1008.93	?				
51	1009.858	1009.85	C II	$2s2p^2\ ^4P_{1/2}$	–	$2p^34S_{3/2}$	]
	1010.005		Fe III	$3d^63P_1$	–	$3d^5(a^4P)4p\ ^3P_2$	]
78	1010.083	1010.00	C II	$2s2p^2\ ^4P_{1/2}$	–	$2p^3\ ^4S_{3/2}$	]
	1010.20 P		Ne VI	$2s^22p\ ^2P_{3/2}$	–	$2s2p^2\ ^4P_{1/2}$	] new wavelength
100	1010.371	1010.28	C II	$2s2p^2\ ^4P_{5/2}$	–	$2p^3\ ^4S_{3/2}$	]
33	1012.411	1012.42	Fe III	$3d^6\ ^3P_0$	–	$3d^5(a^4P)4p\ ^3P_1$	]
	1012.50		S III	$3s^23p^2\ ^3P_0$	–	$3s3p^33P_1$	]
18	1014.42	1014.42*	S II	$3s^23p^3\ ^2D_{5/2}$	–	$3s^23p^24s\ ^2P_{3/2}$	?
44	1015.57	1015.50	S III	$3s^23p^2\ ^3P_1$	–	$3s3p^3\ ^3P_1$	]
36	1015.76	1015.77	S III	$3s^23p^2\ ^3P_1$	–	$3s3p^3\ ^3P_2$	]
71	1017.254	1017.24	Fe III	$3d^6\ ^3H_6$	–	$3d^5(a^4G)4p\ ^3H_6$	
51	1017.745	1017.75	Fe III	$3d^6\ ^3H_5$	–	$3d^5(a^4G)4p\ ^3H_5$	
41	1018.286	1018.29	Fe III	$3d^6\ ^3H_4$	–	$3d^5(a^4G)4p\ ^3H_4$	

Table 1. continued

Peak[1], mW sr^{-1}m^{-2}Å^{-1}	λ_{lit}, Å[2]	λ_{obs}, Å[3]	Line	Transition			Remarks
15	1019.53	1019.54	S II	$3s^23p^3\ ^2D_{3/2}$	–	$3s^23p^24s\ ^2P_{1/2}$	]
22	1019.789	1019.78	Fe III	$3d^6\ ^3D_3$	–	$3d^5(a^4D)4p\ ^3P_2$	]
12	1020.6988	1020.67	Si II	$3s^23p\ ^2P_{1/2}$	–	$3s^25s\ ^2S_{1/2}$	
40	1021.10	1021.08	S III	$3s^23p^2\ ^3P_2$	–	$3s3p^3\ ^3P_1$	]
97	1021.32	1021.32	S III	$3s^23p^2\ ^3P_2$	–	$3s3p^3\ ^3P_2$	]
	1021.561		Fe III	$3d^6\ ^3D_2$	–	$3d^5(a^4D)4p\ ^3P_1$	]
19	1023.7002	1023.73	Si II	$3s^23p\ ^2P_{3/2}$	–	$3s^25s\ ^2S_{1/2}$	]
27	1024.108	1024.20	Fe III	$3d^6\ ^3D_1$	–	$3d^5(a^4D)4p\ ^3P_0$	]
	1025.246		He II	$2s\ ^2S_{1/2}$	–	$4p\ ^2P_{3/2}$	]
(1146)	1025.722		H I	$1s\ ^2S$	–	$3p\ ^2P$	] self-absorbed
	1025.7618		O I	$2s^22p^4\ ^3P_2$	–	$2s^22p^33d\ ^3D_3$	]
63	1026.790	1026.76	Fe III	$3d^6\ ^3G_5$	–	$3d^5(a^4G)4p\ ^3G_5$	]
210	1027.4307	1027.44*	O I	$2s^22p^4\ ^3P_1$	–	$2s^22p^33d\ ^3D_2$	
100	1028.1571	1028.15	O I	$2s^22p^4\ ^3P_0$	–	$2s^22p^33d\ ^3D_1$	
	1030.87		S II	$3s^23p^3\ ^2P_{1/2}$	–	$3s^23p^24s\ ^2D_{3/2}$	]
24	1030.924	1030.92	Fe III	$3d^6\ ^3G_4$	–	$3d^5(a^4G)4p\ ^3G_4$	]
38	1031.34	1031.39	S II	$3s^23p^3\ ^2P_{3/2}$	–	$3s^23p^24s\ ^2D_{5/2}$	]
2465	1031.924	1031.93	O VI	$2s\ ^2S_{1/2}$	–	$2p\ ^2P_{3/2}$	]
	1032.123		Fe III	$3d^6\ ^3F_4$	–	$3d^5(a^4G)4p\ ^3F_4$	]
28	1033.225	1033.27	Fe III	$3d^6\ ^3F_4$	–	$3d^5(a^4G)4p\ ^3F_3$	]
25	1033.298	1033.42	Fe III	$3d^6\ ^3G_3$	–	$3d^5(a^4G)4p\ ^3G_3$	]
22	1033.70		?				
52	1035.768	1035.80	Fe III	$3d^6\ ^3F_3$	–	$3d^5(a^4G)4p\ ^3F_3$	
333	1036.3367	1036.34	C II	$2s^22p\ ^2P_{1/2}$	–	$2s2p^2\ ^2S_{1/2}$	
357	1037.0182	1037.00	C II	$2s^22p\ ^2P_{3/2}$	–	$2s2p^2\ ^2S_{1/2}$	
1482	1037.614	1037.64	O VI	$2s\ ^2S_{1/2}$	–	$2p\ ^2P_{1/2}$	
57	1038.355	1038.36*	Fe III	$3d^6\ ^3F_2$	–	$3d^5(a^4G)4p\ ^3F_2$	
41	1039.2304	1039.22	O I	$2s^22p^4\ ^3P_2$	–	$2s^22p^34s\ ^3S_1$	
44	1040.9425	1040.90*	O I	$2s^22p^4\ ^3P_1$	–	$2s^22p^34s\ ^3S_1$	
39	1041.6876	1041.66*	O I	$2s^22p^4\ ^3P_0$	–	$2s^22p^34s\ ^3S_1$	
17	1043.080	1043.12	N I	$2s^22p^3\ ^2D_{5/2}$	–	$2s^22p^27d\ ^4D_{7/2}$	]
	1043.166		N I	$2s^22p^3\ ^2D_{5/2}$	–	$2s^22p^27d\ ^2F_{7/2}$	]
17	1044.087	1044.09	N I	$2s^22p^3\ ^2D_{3/2}$	–	$2s^22p^27d\ ^2P_{1/2}$	]
	1044.188		N I	$2s^22p^3\ ^2D_{5/2}$	–	$2s^22p^27d\ ^4P_{3/2}$	]
32	1045.766	1045.79	Al IV	$2s^22p^53s\ ^3P_1$	–	$2s^22p^53p\ ^1S_0$	?
21	1049.06	1049.06	S II	$3s^23p^3\ ^2D_{3/2}$	–	$3s^23p^23d\ ^4F_{3/2}$	]
	1049.2		Si VII	$2s^22p^4\ ^3P_1$	–	$2s^22p^4\ ^1S_0$	]
19	1049.82	1049.86	S I	$3s^23p^4\ ^3P_2$	–	$3s^23p^35s^3P_2$	]
27	1050.30	1050.30*	S I	$3s^23p^4\ ^3P_2$	–	$3s^23p^35s\ ^3P_1$	]
16		1050.51	?				
21		1052.22	?				
23	1053.21	1053.23	S II	$3s^23p^3\ ^2P_{5/2}$	–	$2s^22p^24s\ ^4P_{3/2}$	
22		1059.10	?				
25		1059.52	?				
22	1061.245	1061.27	Fe III	$3d^6\ ^3D_1$	–	$3d^5(a^4D)4p\ ^3D_1$	
31	1061.708	1061.74	Fe III	$3d^6\ ^3D_2$	–	$3d^5(a^4D)4p\ ^3D_2$	]
	1061.827		Fe III	$3d^6\ ^3D_1$	–	$3d^5(a^4D)4p\ ^3D_2$	]
21	1062.272	1062.25	Fe III	$3d^6\ ^3D_2$	–	$3d^5(a^4D)4p\ ^3D_3$	]
158	1062.671	1062.66	S IV	$3s^23p\ ^2P_{1/2}$	–	$3s3p^22D_{3/2}$	]
22	1063.309	1063.33	Fe III	$3d^6\ ^3D_3$	–	$3d^5(a^4D)4p\ ^3D_2$	
37	1063.872	1063.87*	Fe III	$3d^6\ ^3D_3$	–	$3d^5(a^4D)4p\ ^3D_3$	
33	1064.611	1064.65	Fe III	$3d^6\ ^3F_2$	–	$3d^5(a^2G)4p\ ^3G_3$	
35		1065.86	?				

Peak[1], mW sr^{-1}m^{-2}Å^{-1}	λ_{lit}, Å[2]	λ_{obs}, Å[3]	Line	Transition			Remarks
	1066.143		Fe III	$3d^6\ ^3G_5$	–	$3d^5(a^4G)4p\ ^3H_6$	]
72	1066.181	1066.12	Fe III	$3d^6\ ^1S_0$	–	$3d^5(a^4D)4p\ ^3P_1$	]
62	1066.629	1066.65	Si IV	$3d\ ^2D_{5/2}$	–	$4f\ ^2F_{7/2}$	
30	1068.19	1068.19	Fe III	$3d^6\ ^3G_4$	–	$3d^5(a^4G)4p\ ^3H_5$	
23	1069.019	1069.04	Fe III	$3d^6\ ^3G_3$	–	$3d^5(a^4G)4p\ ^3H_4$	
22	1070.556	1070.57	Fe III	$3d^6\ ^3G_4$	–	$3d^5(a^4G)4p\ ^3F_4$	
38	1071.746	1071.76*	Fe III	$3d^6\ ^3G_4$	–	$3d^5(a^4G)4p\ ^3F_3$	
289	1072.990	1072.99	S IV	$3s^23p\ ^2P_{3/2}$	–	$3s3p^22D_{5/2}$	
45	1073.520	1073.55	S IV	$3s^23p\ ^2P_{3/2}$	–	$3s3p^22D_{3/2}$	
35	1075.0246	1074.97	Fe III	$3d^6\ ^3G_3$	–	$3d^5(a^4G)4p\ ^3F_2$	
143	1077.13	1077.13*	S III	$3s^23p^2\ ^1D_2$	–	$3s3p^31D_2$	
187	1083.990	1083.99	N II	$2s^22p^2\ ^3P_0$	–	$2s2p^3\ ^3D_1$	
	1084.562		N II	$2s^22p^2\ ^3P_1$	–	$2s2p^3\ ^3D_1$	]
281	1084.580	1084.60	N II	$2s^22p^2\ ^3P_1$	–	$2s2p^3\ ^3D_2$	]
170	1084.913	1084.93	He II	$2s\ ^2S_{1/2}$	–	$5p\ ^2P_{3/2}$	
	1085.529		N II	$2s^22p^2\ ^3P_2$	–	$2s2p^3\ ^3D_1$	]
	1085.546		N II	$2s^22p^2\ ^3P_2$	–	$2s2p^3\ ^3D_2$	]
418	1085.701	1085.71	N II	$2s^22p^2\ ^3P_2$	–	$2s2p^3\ ^3D_3$	]
41	1092.62	1092.64	S I	$3s^23p^43P_2$	–	$3s^23p^3\ 4d\ ^3P_2$	
41	1096.570	1096.58	S II	$3s^23p^3\ ^2D_{3/2}$	–	$3s3p^42P_{1/2}$	
43	1097.237	1097.24	N I	$2s^22p^3\ ^2D_{5/2}$	–	$2s2p^24d^2F_{7/2}$	]
36	1097.31	1097.34	S I	$3s^23p^4\ ^3P_1$	–	$3s^23p^3\ 4d\ ^3P_2$	]
34	1097.74	1097.80	S I	$3s^23p^4\ ^3P_1$	–	$3s^23p^3\ 4d\ ^3P_1$	]
68	1097.96	1098.03	S I	$3s^23p^4\ ^3P_1$	–	$3s^23p^3\ 4d\ ^3P_0$	]
	1098.097		N I	$2s^22p^3\ ^2D_{3/2}$	–	$2s2p^24d\ ^4P_{5/2}$	]
52	1098.247	1098.20	Fe III	$3d^6\ ^3P_2$	–	$3d^5(a^4F)4p\ ^3D_3$	]
	1098.261		N I	$2s^22p^3\ ^2D_{3/2}$	–	$2s2p^24d\ ^2F_{5/2}$	]
37		1098.88	?				
68	1102.32	1102.32*	S II	$3s^23p^3\ ^2D_{5/2}$	–	$3s3p^4\ ^2P_{3/2}$	
1433	1108.150/2	1108.16	O IV	$2s^22p\ ^2P_{1/2}$	–	$2s2p^2\ ^2P_{1/2}$	] 2nd order
105	1108.368	1108.37	Si III	$3s3p\ ^3P_0$	–	$3s3d\ ^3D_1$	]
	1108.794		C I	$2s^22p^2\ ^3P_2$	–	$2s^22p13d\ ^1P_1$	]
51	1108.804	1108.82	C I	$2s^22p^2\ ^3P_2$	–	$2s^22p13d\ ^1F_3$	]
	1109.028/2		O IV	$2s^22p\ ^2P_{3/2}$	–	$2s2p^2\ ^2P_{3/2}$	] 2nd order
69	1109.031	1109.00	C I	$2s^22p^2\ ^3P_0$	–	$2s^22p13d\ ^3D_1$	]
40	1109.233	1109.24	C I	$2s^22p^2\ ^3P_1$	–	$2s^22p13d\ ^3D_1$	] ?
39	1109.836	1109.82	C I	$2s^22p^2\ ^3P_1$	–	$2s^22p12d\ ^1P_1$	]
252	1109.965	1109.91*	Si III	$3s3p\ ^3P_1$	–	$3s3d\ ^3D_2$	]
	1110.169		C I	$2s^22p^2\ ^3P_2$	–	$2s^22p13d\ ^1P_1$	]
51	1110.198	1110.22	C I	$2s^22p^2\ ^3P_2$	–	$2s^22p12d\ ^1F_3$	]
30	1111.010	1111.01	C I	$2s^22p^2\ ^3P_2$	–	$2s^22p12d\ ^3P_3$	]
29	1111.421	1111.42	C I	$2s^22p^2\ ^3P_0$	–	$2s^22p11d\ ^1P_1$	]
36	1111.624	1111.60	C I	$2s^22p^2\ ^3P_1$	–	$2s^22p11d\ ^1p_1$	]
	1111.957		C I	$2s^22p^2\ ^3P_2$	–	$2s^22p11d\ ^1P_1$	]
40	1112.003	1111.99	C I	$2s^22p^2\ ^3P_2$	–	$2s^22p11d\ ^3F_3$	]
32	1112.269	1112.22	C I	$2s^22p^2\ ^3P_0$	–	$2s^22p11d\ ^1D_1$	]
36	1112.472	1112.47	C I	$2s^22p^2\ ^3P_1$	–	$2s^22p11d\ ^3D_1$	]
30	1112.806	1112.79	C I	$2s^22p^2\ ^3P_2$	–	$2s^22p11d\ ^3D_1$	]
	1112.825		C I	$2s^22p^2\ ^3P_2$	–	$2s^22p11d\ ^3F_3$	]
458	1113.228	1113.23	Si III	$3s3p\ ^3P_2$	–	$3s3d\ ^3D_3$	]
34	1113.996	1114.00	C I	$2s^22p^2\ ^3P_1$	–	$2s^22p10d\ ^1P_1$	

Table 1. continued

Peak[1], mW sr^{-1}m^{-2}Å^{-1}	λ_{lit}, Å[2]	λ_{obs}, Å[3]	Line	Transition			Remarks
	1114.332		C I	$2s^22p^2\ ^3P_2$	–	$2s^22p10d\ ^1P_1$	]
	1114.380		C I	$2s^22p^2\ ^3P_2$	–	$2s^22p10d\ ^1F_3$	]
47	1114.457	1114.47	C I	$2s^22p^2\ ^3P_2$	–	$2s^22p10d\ ^3P_1$	]
36	1114.628	1114.64	C I	$2s^22p^2\ ^3P_0$	–	$2s^22p10d\ ^3D_1$	]
36	1114.832	1114.86	C I	$2s^22p^2\ ^3P_1$	–	$2s^22p10d\ ^3D_1$	
33	1115.168	1115.21	C I	$2s^22p^2\ ^3P_2$	–	$2s^22p10d\ ^3D_1$	]
	1115.225		C I	$2s^22p^2\ ^3P_2$	–	$2s^22p10d\ ^3F_3$	]
29	1117.000	1117.02	C I	$2s^22p^2\ ^3P_0$	–	$2s^22p9d\ ^1P_1$	
41	1117.205	1117.22	C I	$2s^22p^2\ ^3P_1$	–	$2s^22p9d\ ^1P_1$	
	1117.542		C I	$2s^22p^2\ ^3P_2$	–	$2s^22p9d\ ^1P_1$	]
47	1117.581	1117.60	C I	$2s^22p^2\ ^3P_2$	–	$2s^22p9d\ ^3P_2$	]
49	1117.724	1117.70	C I	$2s^22p^2\ ^3P_2$	–	$2s^22p9d\ ^3D_3$	]
41	1117.866	1117.88	C I	$2s^22p^2\ ^3P_0$	–	$2s^22p9d\ ^3D_1$	
	1118.070		C I	$2s^22p^2\ ^3P_1$	–	$2s^22p9d\ ^3D_1$	]
40	1118.180	1118.16	C I	$2s^22p^2\ ^3P_1$	–	$2s^22p9d\ ^3F_2$	]
	1118.408		C I	$2s^22p^2\ ^3P_2$	–	$2s^22p9d\ ^3D_1$	]
32	1118.491	1118.49*	C I	$2s^22p^2\ ^3P_2$	–	$2s^22p9d\ ^3F_2$	]
90		1118.90	?				]
27		1119.10	?				]
30	1121.452	1121.47	C I	$2s^22p^2\ ^3P_0$	–	$2s^22p8d\ ^3P_1$	
38	1121.658	1121.65	C I	$2s^22p^2\ ^3P_1$	–	$2s^22p8d\ ^3P_1$	
27	1121.998	1121.91	C I	$2s^22p^2\ ^3P_2$	–	$2s^22p8d\ ^3P_1$	]
47	1122.098	1122.13	C I	$2s^22p^2\ ^3P_2$	–	$2s^22p8d\ ^3P_2$	]
	1122.334		C I	$2s^22p^2\ ^3P_2$	–	$2s^22p8d\ ^3D_3$	]
	1122.438		C I	$2s^22p^2\ ^3P_0$	–	$2s^22p8d\ ^3D_1$	]
599	1122.486	1122.52	Si IV	$3p\ ^2P_{1/2}$	–	$3d\ ^2D_{3/2}$	]
	1122.526		Fe III	$3d^6\ ^5D_4$	–	$3d^5(a^6S)4p\ ^5P_3$	]
	1122.644		C I	$2s^22p^2\ ^3P_1$	–	$2s^22p8d\ ^3D_1$	]
	1122.794		C I	$2s^22p^2\ ^3P_1$	–	$2s^22p8d\ ^3F_2$	]
	1122.985		C I	$2s^22p^2\ ^3P_2$	–	$2s^22p8d\ ^3D_1$	]
42	1123.107	1123.09	C I	$2s^22p^2\ ^3P_2$	–	$2s^22p8d\ ^3F_3$	]
22		1123.44	?				
19		1124.13	?				
265	1124.883	1124.90*	Fe III	$3d^6\ ^5D_3$	–	$3d^5(a^6S)4p\ ^5P_2$	
401	1125.60/2	1125.64	Ne VI	$2s^22p\ ^3P_{3/2}$	–	$2s2p^2\ ^2D_{5/2}$	2nd order
115	1126.728	1126.72	Fe III	$3d^6\ ^5D_2$	–	$3d^5(a^6S)4p\ ^5P_1$	
175	1128.056	1128.05	Fe III	$3d^6\ ^5D_3$	–	$3d^5(a^6S)4p\ ^5P_3$	
190	1128.340	1128.35	Si IV	$3p\ ^2P_{3/2}$	–	$3d\ ^2D_{5/2}$	
191	1128.723	1128.72	Fe III	$3d^6\ ^5D_2$	–	$3d^5(a^6S)4p\ ^5P_2$	
	1129.030		C I	$2s^22p^2\ ^3P_2$	–	$2s^22p7d\ ^1P_1$	]
	1129.141		C I	$2s^22p^2\ ^3P_2$	–	$2s^22p7d\ ^3D_3$	]
145	1129.190	1129.19	Fe III	$3d^6\ ^5D_1$	–	$3d^5(a^6S)4p\ ^5P_1$	]
38	1129.624	1129.60	C I	$2s^22p^2\ ^3P_1$	–	$2s^22p7d\ ^3F_2$	
36	1129.924	1129.92	C I	$2s^22p^2\ ^3P_2$	–	$2s^22p7d\ ^3F_3$	
69	1130.404	1130.40*	Fe III	$3d^6\ ^5D_0$	–	$3d^5(a^6S)4p\ ^5P_1$	
73	1131.194	1131.18	Fe III	$3d^6\ ^5D_1$	–	$3d^5(a^6S)4p\ ^5P_2$	
28	1131.65	1131.60	S II	$3s^23p^3\ ^2P_{3/2}$	–	$3s^23p^24s\ ^2P_{1/2}$	?
40	1131.914	1131.92	Fe III	$3d^6\ ^5D_2$	–	$3d^5(a^6S)4p\ ^5P_3$	
102		1133.68	?				
24	1134.1651	1134.16	N I	$2s^22p^3\ ^4S_{3/2}$	–	$2s2p^4\ ^4P_{1/2}$	
35	1134.4147	1134.39	N I	$2s^22p^3\ ^4S_{3/2}$	–	$2s2p^4\ ^4P_{3/2}$	
45	1134.9801	1134.98*	N I	$2s^22p^3\ ^4S_{3/2}$	–	$2s2p^4\ ^4P_{5/2}$	
24		1135.55	?				
25	1136.51	1136.56	Ne V	$2s^22p^2\ ^3P_1$	–	$2s2p^3\ ^5S_2$	
65	1139.093	1138.97	C I	$2s^22p^2\ ^3P_2$	–	$2s^22p6d\ ^3P_2$	
42	1139.766	1139.82	C I	$2s^22p^2\ ^3P_1$	–	$2s^22p7s\ ^3P_2$	]
	1139.812		C I	$2s^22p^2\ ^3P_2$	–	$2s^22p6d\ ^3D_3$	]
33	1140.357	1140.37	C I	$2s^22p^2\ ^3P_1$	–	$2s^22p6d\ ^3F_1$	
34	1140.641	1140.63	C I	$2s^22p^2\ ^3P_2$	–	$2s^22p6d\ ^3F_3$	
22	1141.272	1141.29	Fe III	$3d^6\ ^1G_4$	–	$3d^5(a^2H)4p\ ^1H_5$	
29	1141.6246	1141.68	C II	$2s2p^2\ ^2D_{5/2}$	–	$2s^24p\ ^2P_{3/2}$	
31	1142.272	1142.34	Fe III	$3d^6\ ^1G_4$	–	$3d^5(a^4G)4p\ ^1H_5$	]
37	1142.464	1142.46*	Fe III	$3d^6\ ^3D_2$	–	$3d^5(a^4G)4p\ ^3F_3$	]
50	1142.955	1143.00	Fe III	$3d^6\ ^3D_3$	–	$3d^5(a^4G)4p\ ^3F_4$	
44	1143.671	1143.67	Fe III	$3d^6\ ^3D_1$	–	$3d^5(a^4G)4p\ ^3F_2$	
38	1145.61	1145.62	Ne V	$2s^22p^2\ ^3P_2$	–	$2s2p^3\ ^5S_2$	
28		1148.69	?				
36	1150.882	1150.80	O III				?
96	1152.1512	1152.15*	O I	$2s^22p^4\ ^1D_2$	–	$2s^22p^33s\ ^1D_2$	
49	1155.99	1156.00	S I	$3s^23p^4\ ^3P_2$	–	$3s^23p^33d\ ^3P_2$	
84	1156.26	1156.27	S I	$3s^23p^4\ ^3P_2$	–	$3s^23p^33d\ ^3P_1$	
37		1160.78	?				
87	1161.35	1161.35*	S I	$3s^23p^4\ ^3P_1$	–	$3s^23p^33d\ ^3P_2$	
72	1161.57	1161.58	S I	$3s^23p^4\ ^3P_1$	–	$3s^23p^33d\ ^3P_1$	
74	1161.72	1161.75	S I	$3s^23p^4\ ^3P_1$	–	$3s^23p^33d\ ^3P_0$	
72	1164.04	1164.02	S I	$3s^23p^4\ ^3P_2$	–	$3s^23p^33d\ ^1D_2$	?
	1168.536	1168.54	N I	$2s^22p^3\ ^2D_{3/2}$	–	$2s^22p^23d\ ^2F_{5/2}$	]
1756	1168.66/2	1168.68	He I	$1s^2\ ^1S_0$	–	$2p\ ^1P_1$	] 2nd order
969	1174.933	1174.88	C III	$2s2p\ ^3P_1$	–	$2p^2\ ^3P_2$	
726	1175.263	1175.24	C III	$2s2p\ ^3P_0$	–	$2p^2\ ^3P_1$	
	1175.590		C III	$2s2p\ ^3P_1$	–	$2p^2\ ^3P_1$	]
2114	1175.711	1175.74	C III	$2s2p\ ^3P_2$	–	$2p^2\ ^3P_2$	]
904	1175.987	1175.98	C III	$2s2p\ ^3P_1$	–	$2p^2\ ^3P_0$	
939	1176.370	1176.37	C III	$2s2p\ ^3P_2$	–	$2p^2\ ^3P_1$	

[1] The numbers in the first column represent the peak intensity of the lines. The continuum background is not subtracted. These entries have been corrected for the instrument spectral response by applying the radiometric calibration. Intensities of EUV lines in the upper solar atmosphere changes on short time scales. Since the various parts of the spectrum were not recorded simultaneously, the numbers in the first column should be used only as rough indications to the relative strengths of the particular transition. Blends normally have no intensity (or wavelength measurement entry) except for some cases where they could partially be separated. The same applies for members of the Lyman series since their line shape is strongly affected by the self-absorption. Blends are indicated in the last column by brackets.

[2] Wavelengths are mostly from the compilation by R.L. Kelly (1987). For lines with blends more than one wavelength is given, including unresolved lines if there is evidence (e.g. from the second order spectrum) that they may contribute to some extent.

[3] The wavelengths were obtained by averaging measurements from two different detector recordings. Lines marked by an asterisk were taken as reference lines for the wavelength calibration. Lines without identification are included as well and indicated by a "?" in Col. 4. Questionable identifications are marked by a "?" in the last column.